NOISE PROPERTIES OF
VERY SHORT GaAs DEVICES

BY

JEAN H. ANDRIAN

A DISSERTATION PRESENTED TO THE GRADUATE
SCHOOL OF THE UNIVERSITY OF FLORIDA
IN PARTIAL FULFILLMENT OF THE REQUIREMENTS
FOR THE DEGREE OF DOCTOR OF PHILOSOPHY

UNIVERSITY OF FLORIDA

1985

TABLE OF CONTENTS

NOISE PROPERTIES OF VERY SHORT GaAs DEVICES

By

Jean H. Andrian

May 1985

Noise properties of n^+ n^- n^+, p^+ p^- p^+, and p^+ n^- p^+ GaAs
structures are investigated. The thickness of the n-type devices are
.24μm, .4μm, and 2.0μm while the p^+ n^- p^+ and p^+ p^- p^+ have a thickness
of .4μm. These very short devices are of interest since they are useful
tools to investigate fundamental phenomena such as ballistic transport
and 1/f noise.

Current-voltage measurements and low frequency noise measurements
at room temperature for every device previously mentioned are
presented. Comparison between the various levels of 1/f noise in the n-
type devices leads to the conclusion that mobility fluctuations are
responsible for noise in these devices, since in the shorter devices
(.24μm and .4μm), the noise level is low. This suggests some carriers
have a near-ballistic transport. The high level of low frequency noise

in the $p^+ n^- p^+$ device suggests the possibility of noise due to traps in this device.

The noise at high frequency and at high electric fields is further investigated on the 1.1μm n-type device.

A step-up transformer is designed to bring the noise of the device to a level above that of the radio frequency preamplifier.

The noise at high electric fields can be explained in terms of velocity fluctuations due to intervalley scattering. The electron drift velocity $v(E)$, and the electron diffusion coefficient $D(E)$ obtained from the measurements by the numerical deconvolution of the I-V characteristic and the noise spectral density, are compared to those obtained by Monte Carlo simulation techniques.

Progress in semiconductor device technology such as the development of the Molecular Beam Epitaxy (MBE) made it possible to fabricate devices with ever decreasing size. The use of compound semiconductors with relatively high carrier mobility such as GaAs to fabricate these small devices has led to the fabrication of low power high-speed devices. Beyond these practical considerations such small structures are useful tools to investigate new models of charge transport for which traditional approaches no longer apply.

If one seeks to use these small devices as part of a detection system like sensors, then the noise performance of the device is very important, since the noise can be a serious limitation on the performance of the system.

Noise studies do not only serve those practical purposes. Low frequency noise measurements may contribute very much to the understanding of the 1/f noise phenomenon. Thermal noise measurements at higher frequencies and higher bias voltages can give useful information about the high electric field behavior of these devices. All these experiments supported with numerical simulations are described in this work.

The organization of the chapters is as follows. In Chapter II a review of previous work on noise measurements of submicron devices is summarized. Measurement procedures of low frequency noise are presented

1

in Chapter III. In Chapter IV experimental results on low frequency noise measurements on n^+ n^- n^+, p^+ p^- p^+, and p^+ n^- p^+ GaAs structures are described. In Chapter V an analysis and discussions of the results of the low frequency noise measurements are presented.

Chapter VI is the beginning of the second part of this work, which investigates the high electric field noise properties of the 1.1μm n^+ n^- n^+ GaAs device. Measurement procedures are described in that chapter. In Chapter VII experimental results are presented. A Monte Carlo simulation method which is used to calculate the electron drift velocity and the electron diffusion coefficient as a function of the electric field is described in Chapter VIII. Chapter IX is devoted to the discussion of the experimental results and numerical calculation of the thermal noise. Finally conclusions and recommendations for further work are presented in Chapter X.

CHAPTER II
PREVIOUS WORK

In the first part of this chapter theoretical work about current-voltage characteristics is briefly described. The second part presents the experimental work on .4μm n^+ n^- n^+ GaAs and .47μm n^+ p^- n^+ performed by R.R. Schmidt [1]. Shur and Eastman [2] used the theory of vacuum tubes to derive a simple model. The current density is given by

$$J = q n v \qquad (2.1)$$

where q is the electronic charge, n is the free electron density and v is the velocity.

The velocity v can be obtained from the energy conservation equation

$$qV_x = 1/2 \ m^* \ v^2 \qquad (2.2)$$

where V_x is the potential of x due to the applied voltage V, and m^* the effective mass of the electron.

The relation between the potential V_x and the electron density is given by Poisson's equation. They arbitrarily set the initial velocity at the cathode and the field equal to zero.

This approach leads to a 3/2 power law $(J \sim V^{3/2})$ for large bias voltages (Child's law) and an 1/2 power law for low bias voltages.

3

The same authors [3] later modified the previous models by introducing a friction term which takes into account the few possible scattering events. Equation (2.2) is then replaced by

$$\frac{d}{dt}(m^* \, v) = q \, E - \frac{m^* \, v}{\tau} \qquad (2.3)$$

where τ is a momentum relaxation time.

Basically both models have been questioned by the fact that the boundary conditions were arbitrarily set. Rosenberg et al. [4] have shown that in the case of very short devices the boundary conditions are very important in modelling the devices.

Holden and Debney [5] with their improved theory of ballistic transport in one dimension, present an interesting approach to the problem. They introduce the fact that the electrons have an initial velocity distribution at the contacts. The method of analysis of the problem is essentially that used for vacuum tubes by Fry [6]. This method is also known as the Langmuir-Fry method. They recognize that, for low bias at least, a potential minimum exists between the electrodes because the cathode contact can supply more electrons to the n$^-$ region than reach the anode. An advantage of this particular formulation is the natural way in which the boundary conditions for the problem are imposed. These are specified by the potential at the anode and the cathode and the total electron injection rates from the n$^+$ contacts, together with the implicit condition of zero electric field at the potential minimum. This situation is depicted in Figure 2.1. x' is the distance from the cathode where the potential minimum occurs and V' is its magnitude.
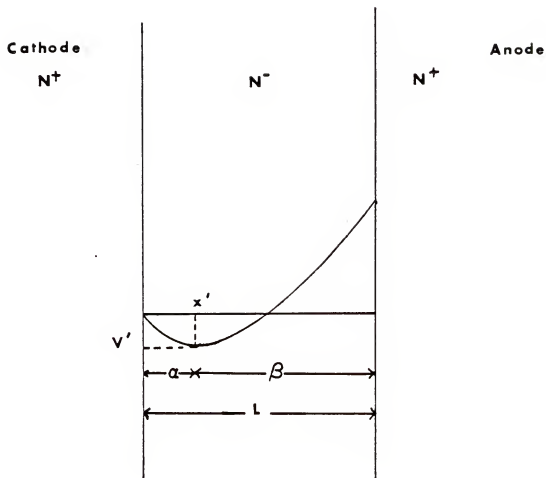
Figure 2.1: Potential profile of
the Holden-Debney model

The problem is then to describe the charge density $\rho(x)$ in the region (α) between the cathode and the potential minimum and in the region (β) between the potential minimum and the anode.

For each region Poisson's equation is solved.

$$\frac{d^2V}{dx^2} = - \frac{\rho(x)}{\varepsilon\varepsilon_0} \qquad (2.4)$$

In the region (α) $\rho(x)$ is the sum of four contributions:

ρ_1: The density of electrons emitted by the cathode which have enough energy to overcome the potential minimium and reach the anode. They have a velocity greater than a critical velocity v_0^1 such that

$$1/2 \; m^* \; v_0^2 - qV' > 0 \qquad (2.5)$$

or

$$v_0 > (\frac{2q}{m^*} \; V')^{1/2} = v_0^1 \qquad (2.6)$$

then

$$\rho_1 = q \int_{v_0^1}^{\infty} \frac{n \; (v_0)}{v} \; dv_0 \qquad (2.7)$$

ρ_2: The density of electrons emitted by the cathode which do not have enough energy to pass the potential minimum. Thus, there are two equally dense streams of electrons passing in opposite directions and having kinetic energies less tha qV' or in other words

$$0 < v_0 < v_0^1 \qquad (2.8)$$

then

$$\rho_2 = 2q \int_0^{v_0'} \frac{n(v_0)}{v} dv_0 \qquad (2.9)$$

ρ_3: The density of electrons emitted from the anode which have enough energy to overcome the potential minimum v'

$$\rho_3 = q \int_{v_0''}^{\infty} \frac{n(v_0)}{v} dv_0 \qquad (2.10)$$

where

$$v_0'' = [\frac{2q}{m^*}(V_a - V')]^{1/2} \qquad (2.11)$$

V_a: Anode voltage.

ρ_4: The background space charge due to ionized donors

$$\rho_4 = -\frac{q}{} N_D \qquad (2.12)$$

For the region (β) the same expressions hold for ρ except for ρ_2 which becomes

$$\rho_2 = 2q \int_{[\frac{2q}{m}(V - V_a)]^{1/2}}^{v_0''} \frac{n(v_0)}{v} dv_0 \qquad (2.13)$$

ρ_2: The density of the electrons emitted from the anode which have enough energy to escape from the anode but not enough to pass the potential minimum.

In the previous expressions of ρ, q is taken as equal to -1.6×10^{-19} C . In each case Poisson's equation is solved by multiplying both sides of equation (2.4) by $2 \frac{dv}{dx}$ and integrating.

We have

$$(\frac{dV}{dx})^2 = -\frac{2}{\varepsilon\varepsilon_0} \int \rho_i \, dV \qquad (2.14)$$

where ρ_i has been described before. In addition to Poisson's equation, the current density equation is needed.

$$j = q \, N \, e^{-\frac{V'}{V_T}} (1 - e^{\frac{V_a}{V_T}}) \qquad (2.15)$$

where $N = N_D^+ \, \overline{v_0}$ and V_T is the thermal voltage, $\frac{kT}{q}$. These equations must be solved self-consistently to obtain the anode voltage V_a for any specified net current density j flowing between the cathode and the anode. According to Holden and Debney, it is difficult to identify the ballistic motion of the electrons by the current-voltage characteristic only. R.R. Schmidt [1] measured the current as a function of the bias voltage and the low frequency noise for different bias currents on .4μm n^+ n^- n^+ and .47μm n^+ p^- n^+ devices.

The I-V characteristic of the n-type is linear up to about 1 volt for 300 and 77K. Neither the $V^{1/2}$ nor the $V^{3/2}$ dependence was observed. He concluded that the theory of Shur and Eastman [3] is not adequate to describe his results. He believed that a more realistic model is that of Holden and Debney which gives a $V^{1.14}$ dependence at high-bias current for a .5μm device. The low bias voltage regime can be explained by the thermionic and diffusion drift model of van der Ziel et

al. [7]. In that model they calculated separately the resistance due to the thermionic emission and due to the diffusion and drift.

For the 1/f noise R.R. Schmidt [1] reported a Hooge parameter α as low as 5.10^{-8} at room temperature for the .4μm n-type device. This value is five orders of magnitude smaller than the value of 6×10^{-3} reported by Hooge et al. [8] for n-type bulk GaAs. The noise measurement for different temperatures (77K and 300K) suggested that the device is not purely ballistic, but the very low value of α suggests near-ballistic transport. The current-voltage characteristic of the n^+ p^- n^+ device is much more complicated than that of the n^+ n^- n^+ device. It shows substantial nonlinearity. There are two regimes with a transition region in between. At low bias, the characteristic is linear with a DC conductance which is temperature dependent and 100 times smaller than that of the n-type device. The high bias regime is temperature independent and is also linear with a larger conductance than the low bias regime. R.R. Schmidt [1] explained the low bias regime as follows. The conductance depends on temperature because the hole concentration does. At high bias the transport is near-ballistic and thus temperature independent as observed in the n-type device. He explained the difference of conductance in the high bias regime (the p-type device has a conductance four times smaller than that of the n-type device) by the fact that in the p-type case, the barrier is higher. The noise picture fits well in the above description. At low bias R.R. Schmidt [1] measured a noisiness factor $S_{\Delta I}(f)f/I^2$ which was 4×10^6 times that for the n-type device value. At high bias the noise is much smaller. This was shown by measurements performed by C.F. Whiteside [9]. The low value of the noise corresponds to the near ballistic

transport suggested for high bias.   In Chapter III, the measurement
procedures of 1/f noise for low impedance devices are described.

CHAPTER III
MEASUREMENT PROCEDURES

3.1 Current Voltage Measurements

In order to measure the DC I-V characteristic of each device, pulsed measurements were done to prevent excess heating which may change and ultimately damage the devices. An HP 214A pulse generator was used to produce pulses of 1μs width with a repetition rate of 100Hz. The set-up is shown in Figure 3.1. The current flowing through the device is then

$$I = \frac{V_1 - V_2}{R_S} \tag{3.1}$$

where R_S is a biasing resistance whose value should be chosen carefully so that reasonable voltages can be measured across the device.

3.2 Noise Measurements

3.2.a Method

The noise measurement procedure is the usual three points measurement:

- A D.C. voltage is applied to the terminals of the device under test.
- A noise calibration source is applied to the terminals of the small signal equivalent resistance of the device.
- No bias voltage is applied to the small signal equivalent resistance of the device.

11
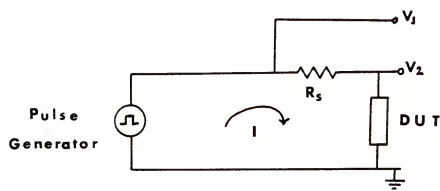
Figure 3.1: Current-voltage
measurement set-up

The fourth information is the magnitude of the calibration itself. This information is sufficient to compute the excess noise of the device.

This is easily understood by analyzing the following block diagram. In position 1 the device is connected to a battery through a calibration resistance R_S. In term of noise, the battery does not contribute at all. Its Norton equivalent is an open circuit. The device under test can be represented by a current source expressing the excess noise in parallel with the small signal resistance of the device itself. The low noise amplifier is modelled as a noiseless amplifier with a voltage gain, a voltage noise source in series at the input and the input impedance and a current noise source in parallel. Finally, the calibration resistance R_S, the input impedance of the amplifier and the device resistance can be lumped together into an equivalent resistance $R_{eq} = R_{dev} \mid\mid R_{in} \mid\mid R_S$ representing an equivalent current noise source $\frac{4k\ T}{R_{eq}}$. The meter reading can be expressed in terms of the power spectral densities of the noise sources as follows:

$$M_1^2 = G^2\ B\ [S_{Vamp} + (S_{Idev} + \frac{4k\ T}{R_{eq}} + S_{Iamp})\ R_{eq}^2] \qquad (3.2)$$

where B is the bandwidth of the spectrum analyzer. In position 2 the device is connected to a calibrated voltage noise source through the same source resistance R_S. The Norton equivalent is a current source in parallel with R_S. The device under test is replaced by a resistor whose resistance is equal to the small signal resistance of the device. This is very important for the case of nonlinear devices.

The expression of the meter reading follows:

$$M_2^2 = G^2 \ B \ [S_{V_{amp}} + (\frac{S_{v_{cal}}}{R_S^2} + \frac{4k \ T}{R_{eq}} + S_{I_{amp}}) \ R_{eq}^2] \tag{3.3}$$

Finally in position 3 the calibration resistance R_S is grounded and the device is replaced by its small signal equivalent. The meter reading is then given by

$$M_3^2 = G^2 \ B \ [S_{V_{amp}} + (\frac{4k \ T}{R_{eq}} + S_{I_{amp}}) \ R_{eq}^2] \tag{3.4}$$

Equations 3.2 and 3.4 yield

$$M_1^2 - M_3^2 = G^2 \ B \ R_{eq}^2 \ S_{I_{dev}} \tag{3.5}$$

similarly 3.4 and 3.4

$$M_2^2 - M_3^2 = G^2 \ B \ R_{eq}^2 \ \frac{S_{V_{cal}}}{R_S^2} \tag{3.6}$$

From equations 3.5 and 3.6 one obtains the excess noise of the device

$$S_{I_{dev}} = \frac{M_1^2 - M_3^2}{M_2^2 - M_3^2} \cdot \frac{S_{V_{cal}}}{R_S^2} \tag{3.7}$$

Every quantity of the right hand side of equation 3.7 is known. This method determines in a unique way the excess noise of the device under test.

3.2.b Description of the Set-Up

In this paragraph, the equipment shown in the block diagram of Figure 3.2 will be described. A Hewlett Packard Model 3582A is used as wave analyzer. This model is a dual-channel spectrum analyzer covering
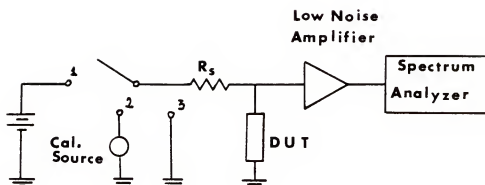
Figure 3.2: Block diagram for the
noise measurement set-up

the frequency range .02Hz to 25KHz, featuring fast Fourier transform for both channels. Its capability of measuring input signals from +30db down to -120db is very important when one deals with small signals like noise.

The low noise preamplifier used is the one called PA1 designed by R.R. Schmidt [1]. The circuit diagram of this amplifier is shown in Figure 3.3. Details of this configuration are well described in R.R. Schmidt's Ph.D. thesis [1]. The main features that make this amplifier very useful for low frequency and low impedance device noise measurement are its extended low frequency response, its high voltage gain of the order of 90db and its relative low input impedance. This low input impedance results from the fact that p n p transistors are used which have low base resistances. The calibration source is provided by the spectrum analyzer itself. It produces a computer generated pseudo random signal. This pseudo random signal has a flat frequency response over the range of the frequency of interest.

In Chapter IV results on current voltage measurements and low frequency noise measurements are presented for $n^+ n^- n^+$, $p^+ n^- p^+$, and $p^+ p^- p^+$ GaAs structures.
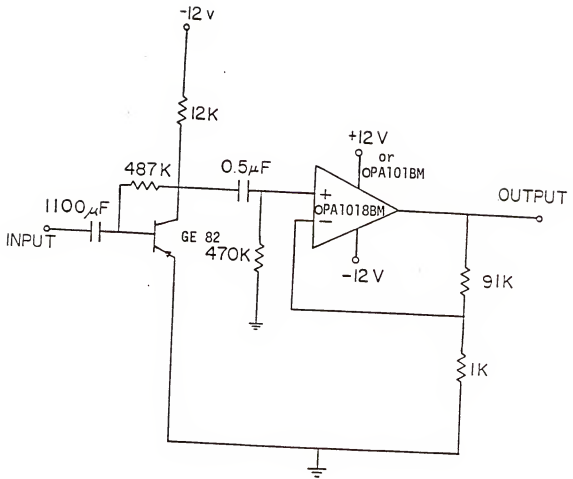
Figure 3.3: Low noise preamplifier

4.1 Current-Voltage Characteristic

4.1.a The n^+ n^- n^+ Device

The diodes are mesa structures with a lightly doped n-type layer sandwiched between heavily doped n^+ layers which serve as contacts. The structure is shown in Figure 4.1. The n^+ regions have a doping density of 10^{18} cm^{-3} while the active region has a doping density of 2 x 10^{15} cm^{-3}. The diameter of the mesa is approximately 100μm. These n-type devices, as well as the others used in the measurements, were manufactured by molecular beam epitaxy at the Cornell University Submicron Research and Resource Facility. The measurements were performed on devices with .24μm, 1.1μm, and 2.0μm thickness. The DC current-voltage characteristic of the 1.1μm n^+ n^- n^+ device at room temperature is shown in Figure 4.2.

At low bias, the characteristic is linear. The device behaves like a resistor. At high bias, around .2V, the conductivity starts to decrease. This corresponds to the transfer of electrons to the upper valley of the conduction band where the electrons have a large effective mass and thus a lower mobility. The 1.1μm device behaves like a bulk n-type GaAs semiconductor. The 2.0μm device has a slightly different doping profile. The n^+ regions have a doping density of 2.10^{18} cm^{-3}. The DC current-voltage characteristic at room temperature is shown in Figure 4.3. The characteristic is linear at bias voltages below .2V.
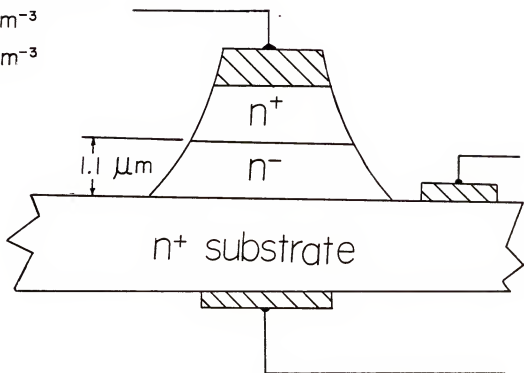
Figure 4.1: 1.1μm n-type device

Figure 4.2: Current-voltage characteristic of the
1.1μm n-type device at room temperature

Figure 4.3: The current-voltage characteristic of
the 2.0 μm n-type device at room temperature

Figure 4.4: Current-voltage characteristic of the
.24μm n-type device at room temperature

For higher bias voltages the characteristic is quadratic, the decrease of conductivity as observed in the 1.1μm device was overshadowed by the effect of space charge injection.

The I.V characteristic of the .24μm device is shown in Figure 4.4. The regime is linear for both low and high bias voltage. This is similar to the .4μm device measured by Schmidt [1]. This may indicate a near ballistic transport.

4.1.b The p^+ p^- p^+ Device

The p-type device has the following structure: a .55μm p^{++} region of 10^{19} cm^{-3} doping density is grown on a p^+ substrate followed by a .55μm p^+ 10^{18} doped region, a .4μm lightly doped p-region and finally a .55μm p^+ 10^{18} and a .55μm p^{++} 10^{19} to serve as contact on top of the mesa. It is really a p^{++} p^+ p^- p^+ p^{++} structure rather than a p^+ p^- p^+. The DC current-voltage characteristic at room temperature is shown in Figure 4.5. The characteristic is linear with a resistance of 1.5Ω. The device behaves like a pure resistance.

4.1.c The p^+ n^- p^+ Device

The structure of the p^+ n^- p^+ device is similar to that of the p^+ p^- p^+ device except that the region .4μm p-region is now replaced by a .4μm n-region with a doping density of 2 x 10^{15} cm^{-3}. The dopent is silicon. The DC current-voltage characteristic at room temperature is shown in Figure 4.6. The characteristic is linear up for bias voltages up to .05V then a 3/2 power low regime is observed up to 1V. Beyond 1V it seems that the characteristic is linear again. However, it is difficult to really assume that just with two experimental data points. It was impossible to go beyond 2V with the available equipment
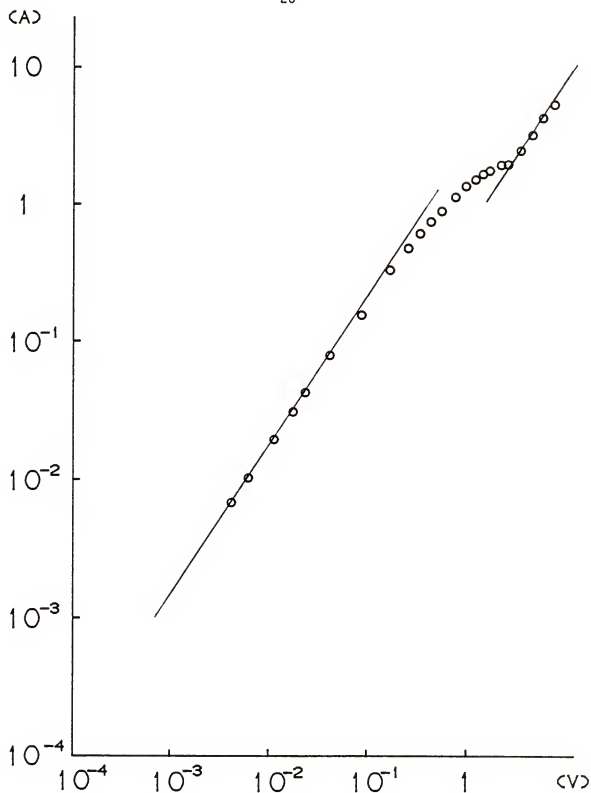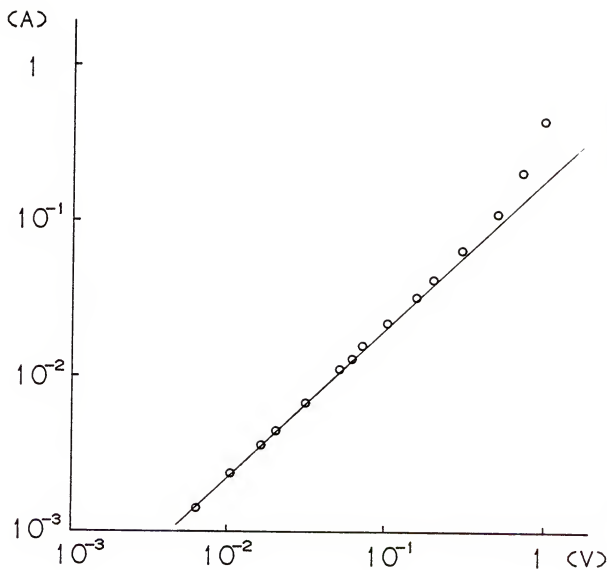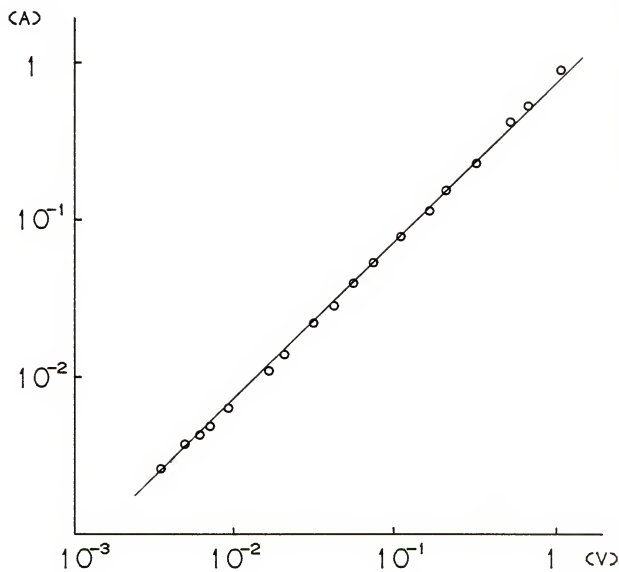
Figure 4.5: The current-voltage characteristic of
the .4μm p-type device at room temperature
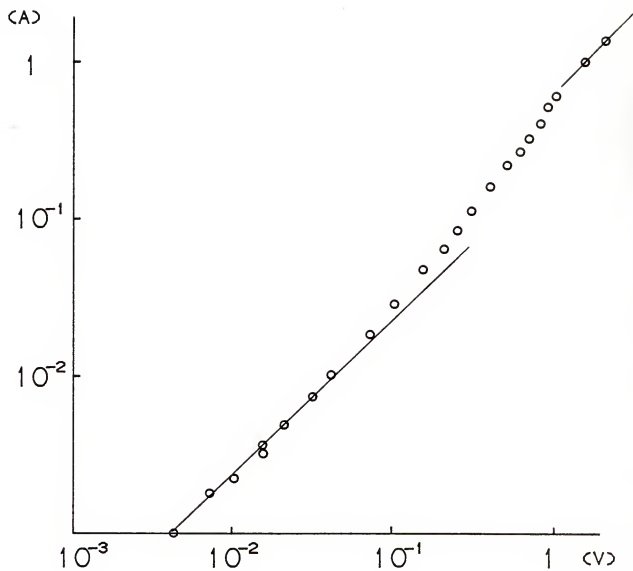
Figure 4.6: The current-voltage characteristic of
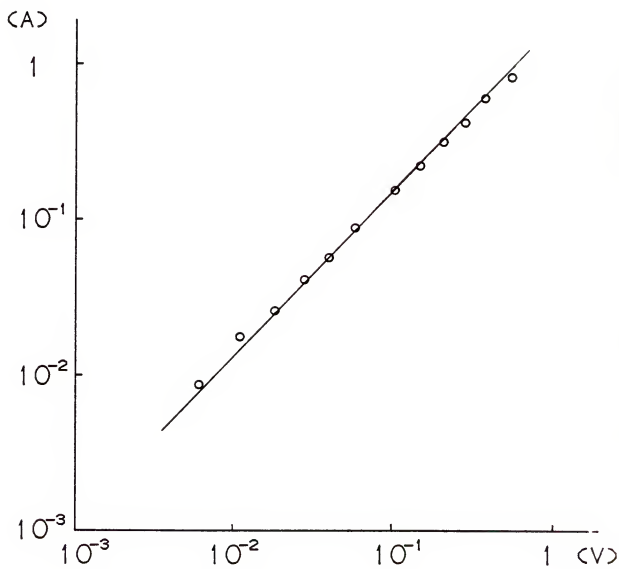the .4 p^+ n^- p^+ device at room temperature

since the pulse generator requires a high impedance load to be able to produce undistorted output signals.

4.2 Low Frequency Noise

4.2.a $n^+ - n^- n^+$ Device

The low frequency excess noise for the 1.1μm device was measured from 1 to 25KHz. The current noise spectral densities S_1 for several bias currents at 300K is shown in Figure 4.7. The frequency dependence of the excess noise is 1/f. From the different bias current levels, the current noise spectral density S_I is proportional to the square of the bias current. This is the expected behavior of the 1/f noise for a device with a linear current-voltage characteristic. The current noise spectral density at room temperature of the 2.0μm device for several bias currents is plotted in Figure 4.8. The frequency dependence is again 1/f at low frequencies up to 1KHz. A steeper slope is then observed beyond 1KHz. The current noise spectral density is proportional to the square of the bias current as expected since the magnitude of the bias currents are still within the linear part of the current-voltage characteristic.

The current noise spectral density at room temperature for the .24μm device is shown in Figure 4.9.

4.2.b The $p^+ p^- p^+$ Device

The low frequency excess noise of the .4μm p-type device was measured from 1Hz up to 25KHz at room temperature. Figure 4.10 shows the current noise spectral density as a function of frequency. The magnitudes of the noise spectral density decreases inversely with the frequency. The spectral density is again proportional to the square of
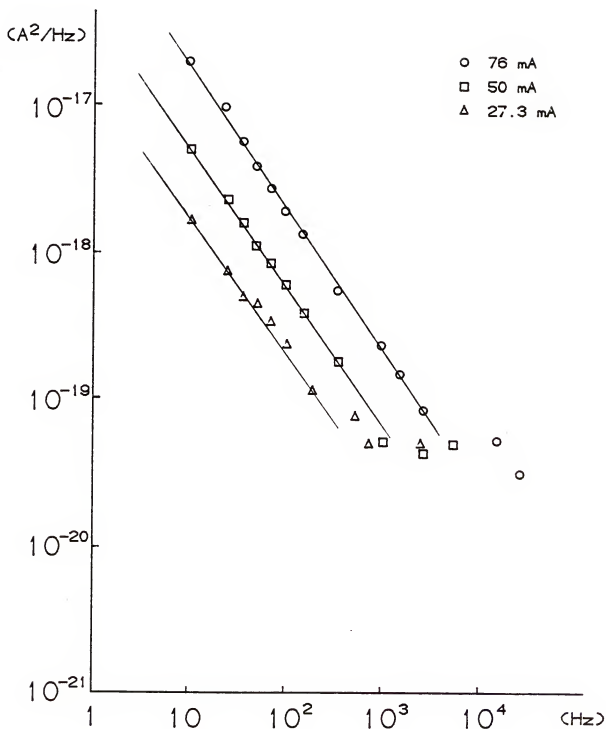
Figure 4.7: Low frequency current noise spectra for the 1.1μm n-type device at room temperature
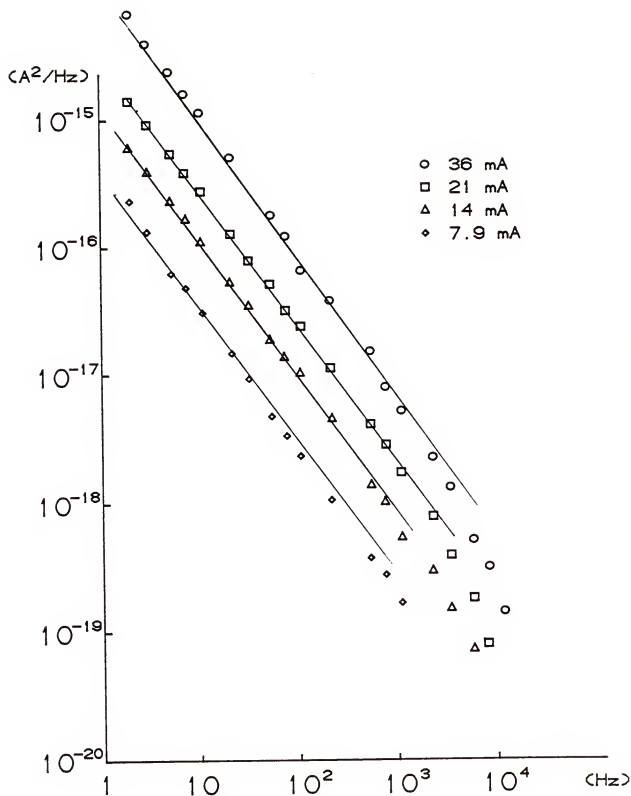
Figure 4.8: Current noise spectra of the 2.0μm
n-type device at room temperature
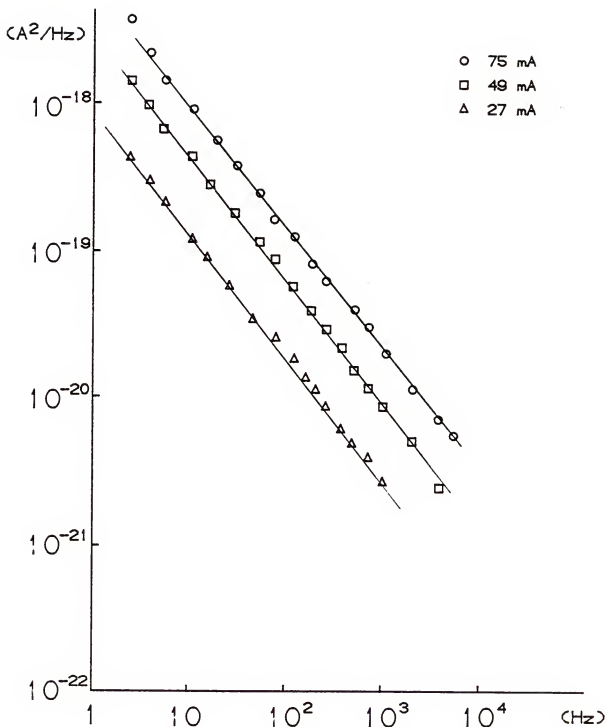
Figure 4.9: Current noise spectra of the .24μm
n-type device at room temperature
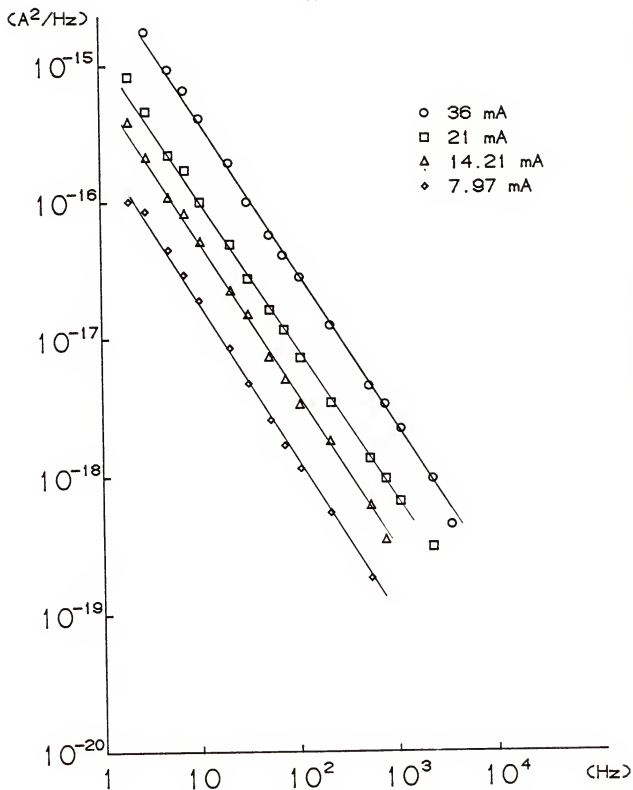
Figure 4.10: Current noise spectra of the .4μm
p+ p- p+ device at room temperature

the bias current as expected since the current-voltage characteristic of the device is linear.

4.2.c The p^+ n^- p^+ Device

The low frequency noise of the .4μm p^+ n^- p^+ device was measured in the same range of frequencies as previously. Figure 4.11 shows the noise spectral density as a function of the frequency at room temperature for different bias currents. The spectra go as 1/f at least for low biases. For low bias currents, the noise is proportional to the square of the bias current, but as the bias current increases, this is not true anymore since the current-voltage characteristic is not linear.

In the next chapter these experimental results will be analyzed and compared with existing theories.
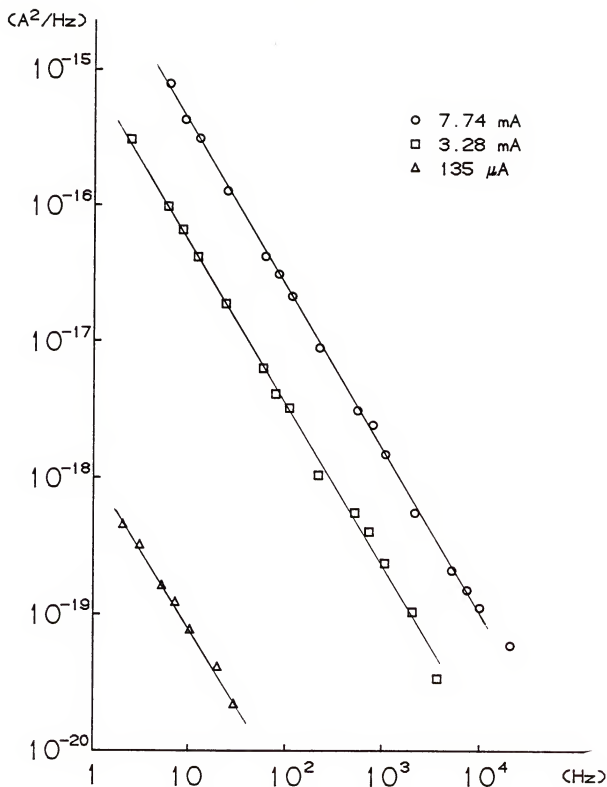
Figure 4.11: Current noise spectra of the .4μm
p+ n- p+ device at room temperature

CHAPTER V
HOOGE'S PARAMETER AND DISCUSSION OF THE RESULTS

5.1 Quantum 1/f Noise Theory

As a starting point we use Handel's formula [10] which expresses the relative spectral density of the scattering cross section as

$$\frac{S\sigma}{<\sigma>^2} = \frac{2\alpha A}{f} \tag{5.1}$$

for low frequency photon emission, one obtains

$$\alpha A = \frac{2\alpha}{3\pi} \left(\frac{\Delta v}{c}\right)^2 \tag{5.2}$$

where $\alpha = 1/137$ is the fine structure coefficient. If the current fluctuation is solely due to mobility fluctuation then one can write

$$\frac{S_I(f)}{I^2} = \frac{S_\mu}{\bar{\mu}^2} \tag{5.3}$$

According to Hooge [11]

$$\frac{S_I(f)}{I^2} = \frac{\alpha_H}{Nf} \tag{5.4}$$

where f is the frequency, I the DC bias current, N the number of carriers, and α_H the Hooge's parameter.

33

Several different scattering mechanisms determine the net mobility of an electron and it is given by

$$\frac{1}{\bar{\mu}} = \sum_i \frac{1}{\mu_i} \tag{5.5}$$

or in terms of spectral density

$$\frac{S_\mu}{\bar{\mu}^2} = \sum_i (\frac{\bar{\mu}}{\mu_i})^2 \frac{S_{\mu_i}}{\mu_i^2} \tag{5.6}$$

From equations (5.3) and (5.4) and for one type of scattering mechanism

$$\frac{S_{\mu_i}}{\mu_i^2} = \frac{\alpha_i}{fN} \tag{5.7}$$

The overall α_H is then

$$\alpha_H = \sum_i (\frac{\bar{\mu}}{\mu_i})^2 \alpha_i \tag{5.8}$$

Kousik [12] has derived expressions of S_{μ_i}/μ_i^2 for different scattering mechanisms, such as impurity scattering polar optical phonon scattering, and acoustical phonon scattering and consequently the individual α_i, by relating the mobility fluctuations to the fluctuation of the scattering cross section given by Handel's formula. This was achieved by considering the fluctuations of the relaxation time associated with each collision process.

5.2 Experimental Determination of α_H for N-Type Device

The next step is now to extract this Hooge's parameter from the experimental measurements. Using again Hooge's empirical formula, we have

$$\alpha_H = \frac{S_I(f)}{I^2} \, f \, N \qquad (5.9)$$

We need to calculate correctly N. Van der Ziel and Van Vliet [13] gave a formula to calculate N, which is also valid for non-homogeneous samples or mesa structures

$$\frac{S_I(f)}{I^2} = \frac{\alpha_H}{f} \frac{1}{AL} \frac{1}{L} \int_0^L \frac{dx}{n(x)} \qquad (5.10)$$

where L is the total length of the device, A the cross sectional area, and $n(x)$ the electron density in the active region. The problem has always been the calculation of the integral since one does not know exactly $n(x)$. Schmidt [1] used an average value $\overline{n}$ which he assumed equal to twice the value of the donor density N_D.

For a device with m layers we have

$$L = m \, L' \qquad (5.11)$$

where L' is the length of one layer.

Substituting in equation (5.11) we have

$$\frac{S_I(f)}{I^2} = \frac{\alpha_H}{fm} \frac{1}{AL'} \frac{1}{L'} \int_0^{L'} \frac{dx}{n(x)} \qquad (5.12)$$

or

$$\alpha_H = \frac{S_I(f)}{I^2} \ f \ m \ N_{eff} \qquad (5.13)$$

where we defined N_{eff} as

$$\frac{1}{N_{eff}} = \frac{1}{AL'} \ \frac{1}{L'} \ \int_0^{L'} \frac{dx}{n(x)} \qquad (5.14)$$

Instead of approximating $n(x)$ by an average value, we computed numerically the carrier concentration profile $n(x)$ and evaluated the integral in equation (5.14). That was done by simultaneously solving Poisson's equation for the entire device and the current continuity equation. The program was developed by S. Tehrani [14]. These carrier concentration profiles are shown in Figure 5.1, 5.2, and 5.3 for the .24, .4, and 1.1 μm devices respectively. The effect of carrier spillover is important in the short devices. For the .24 μm device, the carrier concentration minimum is around 10^{16} cm^{-3} which is ten times the background doping density. The .4 μm device showed a minimum of 3.10^{15} cm^{-3} which is three times the background doping density. Finally the 1.1 μm device is not affected by carrier spillover.

In Table 5.1 α_H computed according to equation (5.13) is listed for the three devices.

Table 5.1: Hooge's parameters for the n-type devices

Length	$\dfrac{S_I}{I^2} \cdot f$	N_{eff}	α_H	m
.24 μm	1. 10^{-15}	3.4 10^7	1.7 10^{-7}	5
.4 μm	1.7 10^{-15}	1.73 10^7	1.5 10^{-7}	5
1.1 μm	2.6 10^{-14}	2.4 10^7	6.2 10^{-7}	1
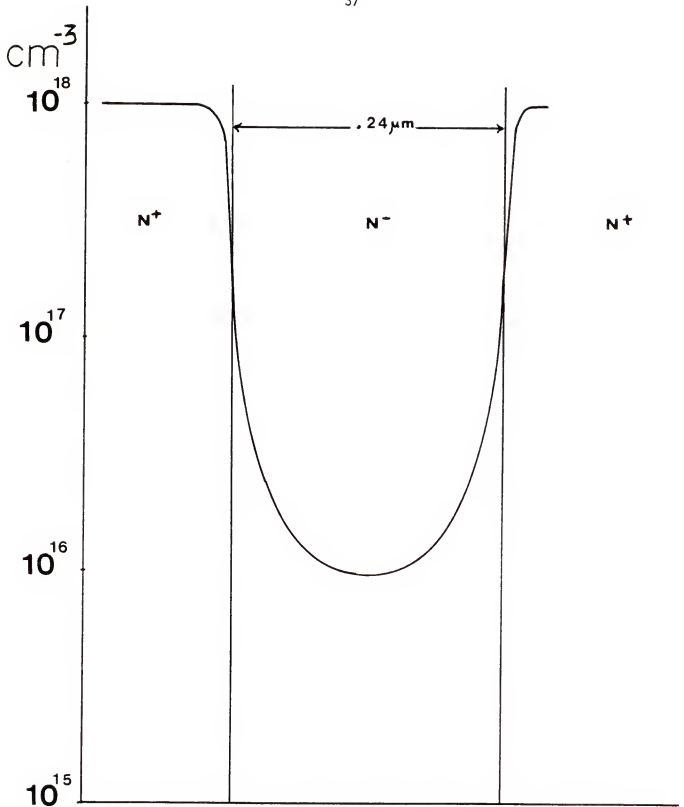
Figure 5.1: Carrier concentration profile
for a .24μm n-type device
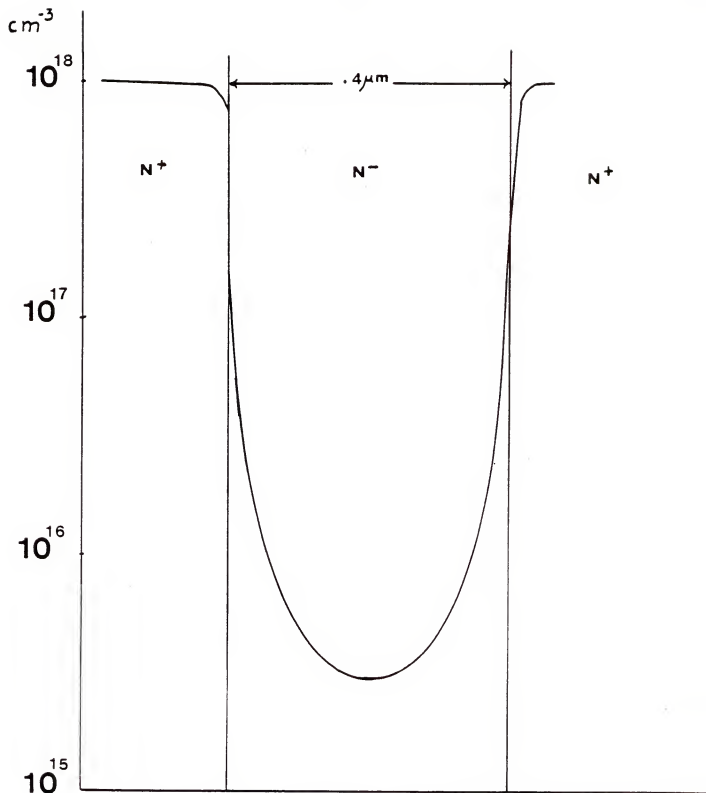
Figure 5.2: The carrier concentration profile
for the .4μm n-type device
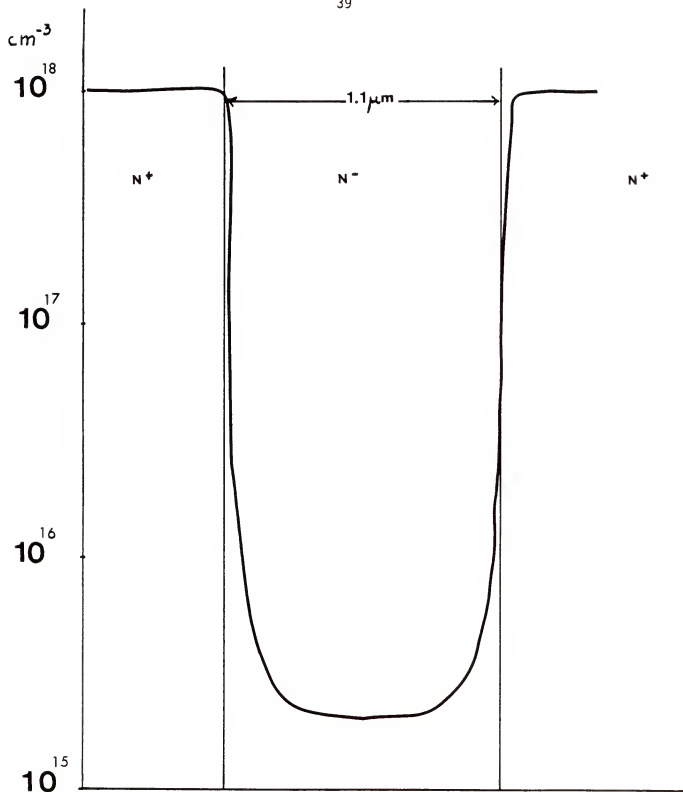
Figure 5.3: Carrier concentration profile of the 1.1μm n-type device

The low values of α_H for the .24μm and the .4μm devices indicate the reduction of noise due to near ballistic transport.

Kousik [12] performed some preliminary calculations on each individual α_i and using equation (5.8) he found $\alpha_H = 2.10^{-8}$ for n type GaAs at room temperature, considering the impurity scattering, acoustical phonon scattering, and polar optical scattering. Comparing this value to those from Table 1, they differ by a factor of ten. This can be explained by some uncertainty in the calculation of N_{eff}, the uncertainty inherent to any measurement or the uncertainty in the material parameters used to compute the theoretical α.

These experimental values and the theoretical one computed by Kousik [12] make us strongly believe that in this case the mobility fluctuation is responsible for the 1/f noise in these samples and that can be understood by using Handel's theory [10]. The same calculation has been carried out for the 2.0 μm n-type device.

The value obtained for α_H is

$$\alpha_H = 6.2 \ 10^{-5} \tag{5.15}$$

This value is three orders of magnitude larger than the theoretical value. This can not be explained by the quantum 1/f noise theory. This device may have a different source of noise other than the fundamental noise due to mobility fluctuation. A closer look to the spectrum may suggest the possibility of generation-recombination noise since the spectrum show $1/f^2$ slope beyond 1 kHz.

5.3 The $p^+ p^- p^+$ Device

From the data, we obtained a value of α_H

$$\alpha_H = 2.6 \ 10^{-5} \tag{5.16}$$

for the .4 μm p-type device at room temperature. Even though the theoretical value of α_H for a p-type GaAs material has not yet been calculated, this experimental value is not likely to be explained by the quantum 1/f noise theory. One has to consider other possible sources of noise. Contacts on p-type epilayer are not as good as those of teh n-type one, and these may give rise to a source of 1/f noise.

5.4 The $p^+ n^- p^+$ Device

The value of α_H in this case is

$$\alpha_H = 2.5 \ 10^{-4} \tag{5.17}$$

which is again too high to be explained by the quantum 1/f noise theory. This value is even ten times larger than the value for the $p^+ p^- p^+$ device which is thought to produce contact noise. A closer comparison with the previous work done by Schmidt [1], however, reveals that the noise has a similar magnitude to that of the 0.47 μm $n^+ p^- n^+$ device. Schmidt [1] did not calculate α_H, rather he used the quantity $(S_I/I^2)f$. An assumption that the noise behaves like 1/f would give an α_H of 1.4 10^{-4}.

The $n^+ p^- n^+$ and the $p^+ n^- p^+$ devices are not only similar with respect to low frequency noise, but also with respect to current-voltage

characteristic. Both exhibit a linear regime at low voltages, a faster increase in conductivity and another linear regime beyond 1V. That second linear regime is not obvious though for the .4 μm p^+ n^- p^+ device. As in the n^+ p^- n^+ case, we can explain the noise in terms of trap filling noise. This type of noise would easily overshadow true 1/f noise.

5.5 Conclusion

We believe that the results from Section 5.2 are a real step toward the understanding of the 1/f noise phenomenon. In that section we established two major facts: first, the Hooge's parameter does not really depend on the length of the device for devices with $L \lesssim 1$ m. Second, for these devices, the experimental values for α_H are comparable to the theoretical ones based on the theory of quantum 1/f noise. There is one order of magnitude difference but that is easily accounted for by the uncertainties we have already discussed. In that respect, the measurements have been conclusive to the understanding of the fundamental 1/f phenomena. This work really establishes the idea that 1/f noise in semiconductors can be explained by mobility fluctuation using Handel's theory [10] as elaborated by Kousik and Van Vliet [12]. The lack of success with the p^+ p^- p^+ device was explained in Section 5.3. The 2.0 μm n-type device, the n^+ p^- n^+, and the p^+ n^- p^+ devices have different noise mechanisms in addition to 1/f noise.

CHAPTER VI
MEASUREMENT PROCEDURES FOR PULSED NOISE MEASUREMENTS

The noise measurement in this part is completely different from the method used in the first part of this work. A general description of the method is given in the first paragraph then a detailed description of the equipment used is given thereafter.

6.1 Experimental Method

The block diagram of the experimental set-up is shown in Figure 6.1. A pulsed bias method was used to avoid excessive Joule heating and possible destruction of the device at high electric fields. The pulse generator is synchronized with a switch at the input of the power detector so that one only measures the noise when the bias is applied. Bareikis et al. [15] have used this method before, however, a detailed description of the step-up transformer method, suggested by Dr. van der Ziel, at the input of the amplifier is given here. This network is very important because the device has a very low impedance ($<1\Omega$) compared to the 50Ω input impedance of the amplifier. As a consequence, the device noise would drown in the amplifier noise without a step-up network.

6.1.a Step-Up Transformer

Since the amplifier has a noise equivalent resistance of 60Ω and the device, a resistance less than 1Ω, a tuned circuit is needed to increase the resistance seen by the amplifier. The noise equivalent circuit is shown in Figure 6.2, where r is the series resistance of the

43
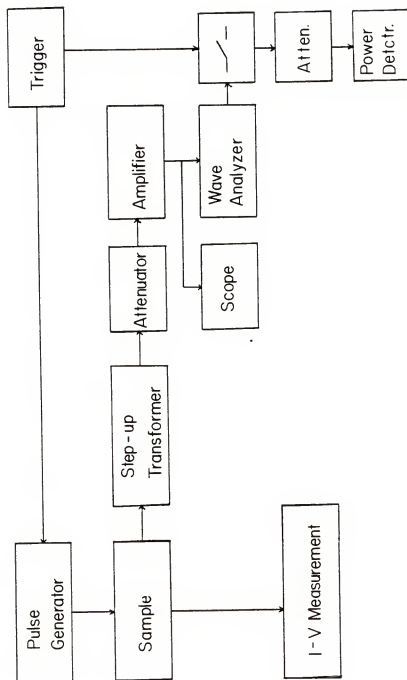
Figure 6.1: Block diagram of the experimental set-up
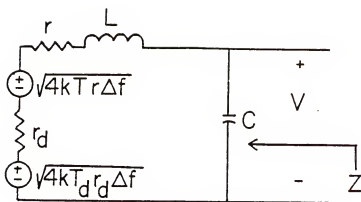
Figure 6.2: Noise equivalent circuit of the
step-up transformer

inductor, r_d the device small signal resistance, and $\sqrt{4kTr\Delta f}$ and $\sqrt{4kTr_d\Delta f}$ (k is the Boltzmann constant) are the thermal noise sources associated with r and r_d respectively.

The impedance at the terminals is given by

$$z = \frac{j\omega L + r + r_d}{1 - \omega^2 CL + j\omega C\ (r + r_d)} \tag{6.1}$$

If one operates at the tuning frequency $\omega_0 = \frac{1}{\sqrt{LC}}$ and if one chooses ω_0 so that $r + r_d \ll |j\omega_0 L|$, then

$$z \approx \frac{L}{C} \cdot \frac{1}{(r + r_d)} \tag{6.2}$$

The spectral density S of the AC open-circuited voltage fluctuations at the output of the network is

$$S = 4k(T_0 r + T_d r_d)\ \left| \frac{\frac{1}{j\omega_0 C}}{\frac{1}{j\omega_0 C} + r + r_d + j\omega_0 L} \right|^2 \tag{6.3}$$

where T_0 is the inductor temperature and T_d the device temperature. Carrying out the algebra and again using the fact that $\omega_0^2 CL = 1$, equation (6.3) becomes

$$S = 4k\ (T_0 r + T_d r_d)\ \frac{L}{C}\ \frac{1}{(r + r_d)^2} \tag{6.4}$$

The condition for "up" transformation of the noise equivalent resistance of the device is easily derived from equation (6.4) if one neglects r. Then S becomes

$$S = 4KT_d \frac{L}{Cr_d} \qquad (6.5)$$

"Up" transformation takes place if

$$\frac{L}{Cr_d} > r_d \text{ or } \frac{L}{C} > r_d^2 \qquad (6.6)$$

For the series resonance step-up transformer, it holds that

$$\frac{L}{C} = r_d^2 Q^2 \qquad (6.7)$$

where Q is the quality factor of the transformer. Hence, condition (6.6) is fulfilled as long as Q > 1. However, a high Q circuit has a narrow passband; therefore transformers for each frequency of interest (11 and 17MHz) were built.

6.1.b Determination of the Series Resistance of the Inductor

If one replaces the device by a short circuit, one obtains

$$S_1 = 4KT_0 \frac{L}{Cr} \qquad (6.8)$$

Next, a known resistance (r_0) is used. Equation (6.4) gives

$$S_2 = 4kT_0 \frac{L}{C(r + r_0)} \qquad (6.9)$$

Equations (6.8) and (6.9) yield

$$\frac{S_1}{S_2} = 1 + \frac{r_0}{r} \qquad (6.10)$$

From equation (6.10) one obtains the value of the series resistance r of the inductor at the tuning frequency.

6.1.c Determination of the Device Resistance with Noise Measurement

The actual device is then placed in series with the inductor. In thermal equilibrium with both the device and the inductor at room temperature T_0, one finds

$$S_3 = 4 \ k \ T_0 \ \frac{L}{C} \ \frac{1}{(r + r_d)} \tag{6.11}$$

Equations (6.9) and (6.11) give

$$\frac{S_2}{S_3} = \frac{r + r_d}{r + r_0} \tag{6.12}$$

From equation (6.12) one can calculate the value of r_d.

6.1.d Noise Measurement with Bias Applied

All previous calculations are valid under thermal equilibrium conditions. However, one is interested in the high field behavior of the noise so one needs to include a biasing circuit in the previous model. The circuit is shown in Figure 6.3 and the noise equivalent circuit circuit in Figure 6.4 Let $V_s = \sqrt{4kT_0R_s\Delta f}$, $V_d = \sqrt{4kT_dr_d\Delta f}$, and $V_r = \sqrt{4kT_0r\Delta f}$. Possible excess noise of the device is taken into account by using the noise temperature T_d in the expression for V_d. A simple analysis of the circuit gives for the voltage fluctuations at the AC open-circuited output terminals at resonance frequency ω_0

$$V = \frac{[r_d(V_s - V_r) + R_s(V_d - V_r)]}{j\omega_0C(R_sr + R_sr_d + rr_d)} \tag{6.13}$$
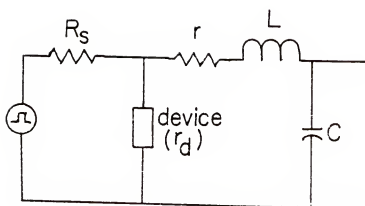
Figure 6.3: The step-up transformer with the
DUT including the pulse bias network
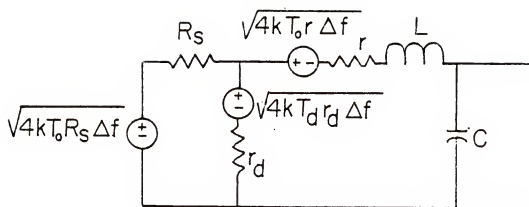
Figure 6.4: Noise equivalent circuit of the step-up
transformer with the DUT including the
bias network

Since the noise sources are not correlated, the mean cross-products $\overline{V_d V_s}$, $\overline{V_s V_r}$, and $\overline{V_d V_r}$ vanish. Hence one obtains

$$S(\omega_0) = \frac{L}{C} \frac{r_d^2(S_{V_r} + S_{V_s})}{(R_s r + R_s r_d + r_d r)^2} + \frac{L}{C} \frac{R_s^2(S_{r_d} + S_{V_r})}{(R_s r + R_s r_d + r_d r)^2}$$

$$\tag{6.14}$$

$$+ \frac{L}{C} \frac{2\, r_d R_s S_{V_r}}{(R_s r + R_s r_d + r_d r)}$$

Since $r_d \ll R_s$ and $r \ll R_s$ ($R_s \approx 50\Omega$), terms with r_d^2 and $r_d R_s$ in the numerator are dropped. Equation (6.14) becomes

$$S(\omega_0) = \frac{L}{C} \frac{1}{r_d^2} \frac{S_{V_r} + S_{V_d}}{(1 + \frac{r}{r_d})^2} \tag{6.15}$$

with $S_{V_r} = 4kT_0 r$ and $S_{V_d} = 4kT_d r_d$. Equation (6.15) can be written as

$$S(\omega_0) = 4k \frac{L}{C} \frac{1}{r_d^2(1 + \frac{r}{r_d})^2} (T_0 r + T_d r_d) \tag{6.16}$$

Equations (6.8) and (6.16) yield

$$\frac{S_1}{S} = \frac{r_d^2(1 + r/r_d)^2\ T_0}{(T_0 r + T_d r_d)} \tag{6.17}$$

or

$$T_d r_d + T_0 r = \frac{S}{S_1} \frac{r_d^2(1 + r/r_d)^2\ T_0}{r} \tag{6.18}$$

The noise equivalent resistance of the device is defined as

$$R_n = \frac{T_d r_d}{T_0} \tag{6.19}$$

From equation (6.18) one obtains

$$R_n = \frac{S}{S_1} \cdot \frac{r_d^2(1 + r/r_d)^2}{r} - r \tag{6.20}$$

Equation (6.20) will be used to calculate the equivalent resistance as a function of the bias voltage. Before presenting the experimental results in Chapter VII, the equipment used will be briefly discussed in the next section.

6.2 Description of the Equipment

6.2.a The Spectrum Analyzer

The spectrum analyzer used was the HP 853A/8558A system. The HP 853A is the spectrum analyzer display and the HP 8559A is the spectrum analyzer itself. The HP8559A spectrum analyzer employs harmonic mixing to cover a measurement range of 10MHz to 21GHz in six frequency bands.

It can display frequency spans as narrow as 100KHz, and as wide as 9GHz. The HP 8559A can be used to measure signals over an amplitude range of -111dBm to +30dBm.

6.2.b The High-Frequency Preamplifier

The high-frequency preamplifier used in this experiment was a two-stage cascode-pair JFET. This configuration provides good bandwidth with reasonable gain. The bandwidth is enhanced by the use of 3μH in series with the load resistance. It has a gain of 30dB and a -3db frequency of 30MHz. This amplifier was designed by C.F. Whiteside [9]. The circuit diagram is shown in Figure 6.5. A radio frequency amplifier model QB-258 by Q-Bit Corporation was cascaded to the previous amplifier.

In Chapter VII the experimental results will be presented.
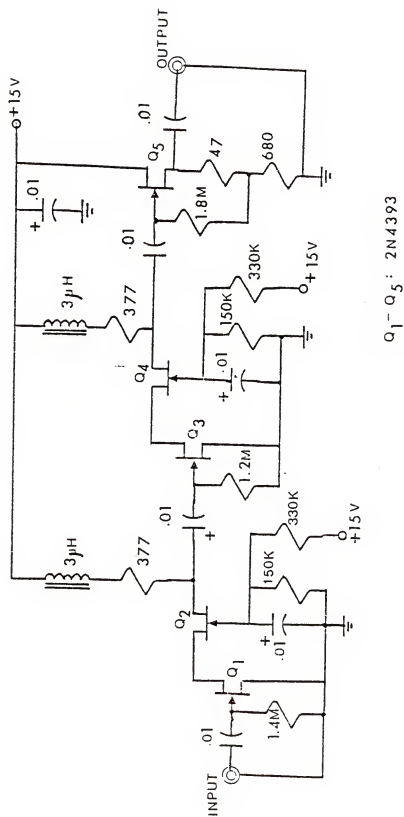
Figure 6.5: High frequency preamplifier

$Q_1 - Q_5$: 2N4393

CHAPTER VII
EXPERIMENTAL RESULTS

Measurements were performed on the 1.1μm n-type device at room temperature at 11 and 17MHz. It was pulsed biased up to 1V. The device resistance measured by noise measurement as described earlier, gave a value of r_d = (.65 ± .06Ω), which is very close to the DC measurement performed during the current-voltage characteristic measurement.

Equation (6.20) from Chapter VI is used to calculate the noise equivalent resistance R_n of the device. In Figure 7.1 R_n is plotted as a function of the applied voltage for T_0 = 300K and f_0 = 11.0 MHz and f_0 = 17.0 MHz. For bias voltages up to .2V the measured value of R_n is equal to the small signal resistance of the device r_d, within the experimental error. For bias voltages above .2V, R_n increases sharply with the voltage applied. These results will be compared to numerical simulation using the Monte Carlo method. This will be the subject of the next two chapters.
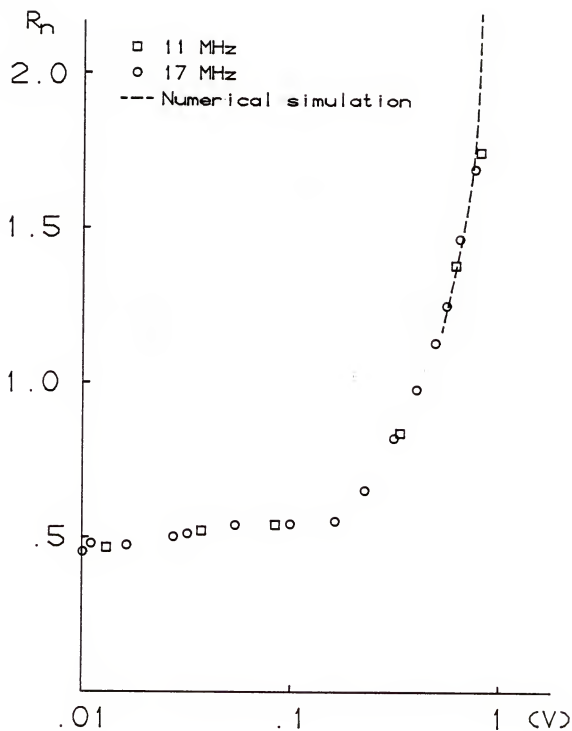
Figure 7.1: Noise equivalent resistance as a
function of the applied voltage

CHAPTER VIII
MONTE CARLO SIMULATION

8.1 Introduction

In order to calculate transport coefficients such as electron mobility for a given applied external field one has to determine the distribution function. The distribution function changes in response to external driving fields, the perturbed distribution function is governed by the appropriate Boltzmann equation, and hence solution of this Boltzmann equation provides a theoretical description of the behavior of the system. Ideally, the Boltzmann equation can be solved by analytical means; and then one has an explicit mathematical formula for properties of the electron system in terms of the governing parameters and variables: for example, mobility versus magnetic field as a function of effective masses and electron-lattice coupling constants [16]. This is possible, however, only for some particular cases of high symmetry and simplicity, which seldom occur in practice.

Simulation techniques have been developed in theoretical physics and engineering to avoid these difficulties. The Monte Carlo method is one of these simulation techniques which proved to be immensely powerful in electron transport theory.

Basically, a Monte Carlo transport simulation consists of modeling the motion of an electron as a sequence of free flights (in an applied field) interrupted by collisions (or scatterings). Between collisions, the electron obeys classical laws of motion determined from the band

structure (effective mass and nonparabolicity) of the material. The collisions are regarded as random events whose probabilities are known functions of energy. The duration of a free flight, the kind of scattering process, and the change in momentum produced by a scattering are determined using numbers produced by a pseudo random number generator usually available on the computer itself. In effect this method produces a numerical solution to the Boltzmann transport equation for a specified set of scattering processes and material parameters [17]. Figure 8.1 shows the main steps in a Monte Carlo simulation: A carrier is initialized by giving a momentum P_0 with a lattice temperature T. The carrier then accelerates freely under an applied field F until it is determined that an interaction has occurred; this determination is based on total scattering rate as a function of carrier energy and on a pseudo random number selected at the beginning of the free flight. After a free flight, another pseudo random number is selected; this number and the individual scattering rates determine which of various interactions occurs. Once a scattering mechanism has been selected, additional pseudo random numbers determine the state of the carrier for the next free flight. These steps (free flight ended by a scattering event) are repeated until a specified number N of interactions has occurred or until a specified time has elapsed. In fact, the history of an electron is followed for a very long time T and each parameter is averaged in time. In the steady state case, this time average is equal to the ensemble average. Each of these steps will be discussed more in detail in the following paragraphs.
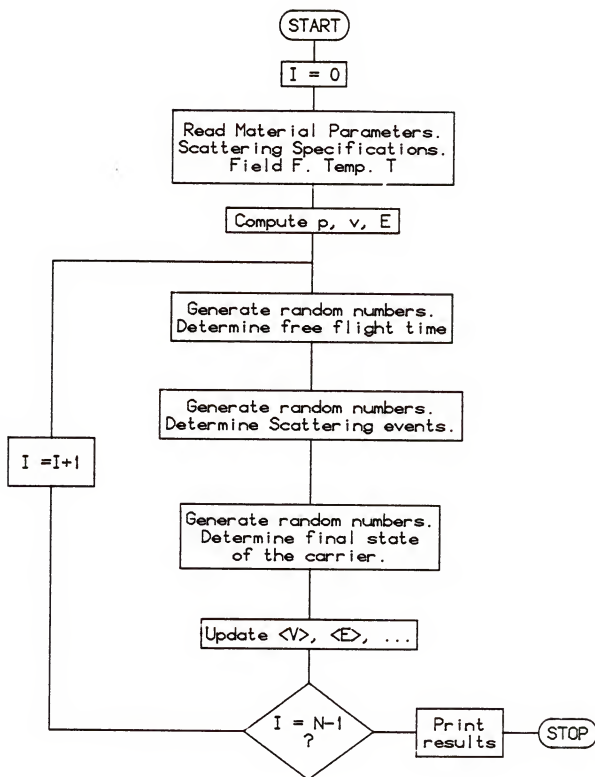
Figure 8.1: Flow chart for Monte Carlo simulation

8.2 General Method

8.2.a Generation of Random Numbers with Given Distributions

Usually parameters like free flight time between collisions are random variables whose probability distribution functions are known. It is convenient to express those random variables as a function of a pseudo random number provided by the computer. These random numbers have usually a uniform distribution between 0 and 1. The transformation goes as follows:

Let r be the pseudo random number and f(r) its probability density function. In this case f(r) = 1 for r E [0, 1] and f(r) = 0 elsewhere.

Let θ be the random variable representing a certain physical quantity and p(θ) its probability density function. We map the pseudo random number r to the distribution function of the physical quantity θ as follows:

$$P\{r' < r\} = P\{\theta < \theta_r\} \tag{8.1}$$

or

$$\int_0^r f(r')dr' = \int_0^{\theta_r} p(\theta)d\theta \tag{8.2}$$

Since f(r) = 1   r E [0, 1]

$$r = \int_0^{\theta_r} p(\theta)d\theta \tag{8.3}$$

From equation (8.3), θ_r can be expressed as a function of the pseudo random number r. This method is used to generate quantities such as free flight time, scattering angle. The transformation resulting from equation (8.3) is sketched in Figure 8.2.

8.2.b Initial Conditions

In the steady state situation, the time of simulation must be long enough so that the initial conditions of the electron motion do not influence the final results. The choice of a "good" time of simulation is a compromise between the need for ergodicity and the request to save computer time [18]. If a highly improbable value of the wave vector k of the electron is chosen, the first part of the simulation can be strongly influenced by this unappropriate choice.

A common practice is to choose as initial energy $k_B T$ where k_B is the Boltzmann constant and T the lattice temperature and deduce from that the initial wave vector k_0 as

$$|\vec{k}_0| = \frac{1}{\hbar} (2m^* k_B T)^{1/2} \tag{8.4}$$

8.2.c Electron Motion

In a simple semiconductor electrons or holes are considered as free particles with effective mass m^* and a dispersion law

$$\frac{\hbar^2 k^2}{2m^*} = \gamma(\varepsilon) \tag{8.5}$$

In the case of a parabolic band which is considered here $\gamma(\varepsilon) = \varepsilon$ where ε is the energy of the carrier.

The effective mass m^* is usually considerably smaller than the free-electron mass $m_0 = 9.1 \ 10^{-31}$ kg. In the case of GaAs it is necessary to describe the electron with two different effective masses.

Between collisions the electron obeys the law of motion
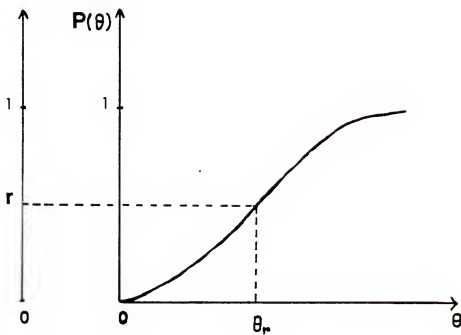
Figure 8.2: Generation of stochastic variable
θ with a given distribution function

$$\hbar \frac{d\vec{k}}{dt} = - e\vec{F} \qquad (8.6)$$

where -e is the electron charge, $\vec{F}$ the electric field. If the electric field $\vec{F}$ is parallel with the k_z-axis, we have the situation shown in Figure 8.3.

If Δt is the drifting time, equation (8.6) can be rewritten as

$$\vec{k}_f(t) = \vec{k}_i - \frac{e\vec{F}}{\hbar} \Delta t \qquad (8.7)$$

where $\vec{k}_i$ is the value at the start of the electron flight and k_f is the value at the end of the flight.

Since the k-space of the electron is symmetric about the electric field $\vec{F}$, it is useful to have an equivalent two-dimensional (k_ρ, k_z) -space where $k_\rho = (k_x^2 + k_y^2)^{1/2}$ instead of the three-dimensional (k_x, k_y, k_z) [19]. Hence the initial state would be (k_ρ, k_{z_i}) and the final state (k_ρ, k_{z_f}) and only the z-component of equation (8.7) needs to be considered. So

$$k_{z_f} = k_{z_i} + \frac{eF}{\hbar} \Delta t \quad ; \qquad (8.8)$$

since $\vec{F} = (0, 0, -F)$, each free flight is terminated by a scattering. Since there are several competing mechanisms the appropriate scattering mechanism is chosen by another Monte Carlo procedure. The free flight duration Δt has to be chosen by a Monte Carlo procedure too. These will be discussed in the next paragraph.
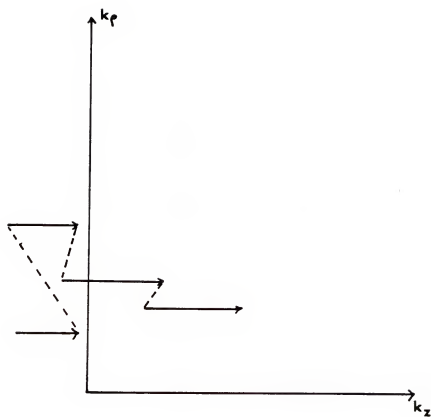
Figure 8.3: Electron motion in momentum space

3.2.d Flight Duration and Choice of Scattering Mechanism

Each scattering mechanism is characterized by a transition rate $S_n(\vec{k}, \vec{k}')$ from the state $\vec{k}$ to the state $\vec{k}'$. The subscript n denotes an individual scattering process and can take values n = 1, 2, ..., N if there are N mechanisms considered. The total scattering rate from the state $\vec{k}$, due to the n-th process, is

$$\lambda_n(\vec{k}) = \int S_n(\vec{k},\vec{k}') \, d\vec{k}' \qquad (8.9)$$

So, the total scattering rate, due to all processes, is

$$\lambda(\vec{k}) = \sum_{n=1}^{N} \lambda_n(\vec{k}) \qquad (8.10)$$

where $\vec{k}$ is a function of time. Usually the total scattering rates are only functions of $k = |\vec{k}|$, so $\lambda(\vec{k})$ is easily transformed to $\lambda(E)$.

Let assume that the electron drifts for a time t before being scattered and that this time consists of n tiny increments Δt_1, Δt_2, Δt_n. The probability of the electron being scattered, within the time interval Δt_i, is $\lambda(\vec{k}) \Delta t_i$, where $\lambda(\vec{k})$ is the total scattering rate defined by equation (8.10). The probability that there will not be any scattering during Δt_i is $(1 - \lambda(\vec{k}) \Delta t_i)$. Since those are independent events, the overall probability of an electron not having any scattering during a time t is then

$$P(t) = \prod_{i=1}^{n} (1 - \lambda(\vec{k}) \Delta t_i) \qquad (8.11)$$

or

$$\ln \{P(t)\} = \sum_{i=1}^{n} \ln \{(1 - \lambda(\vec{k}) \Delta t_i)\} \qquad (8.12)$$

Since $\lambda(\vec{k}) \, \Delta t_i \ll 1$

$$\ln \left\{(1 - \lambda(\vec{k}) \, \Delta t_i)\right\} \simeq - \lambda(\vec{k}) \, \Delta t_i \tag{8.13}$$

and

$$\ln \left\{P(t)\right\} = - \sum_{i=1}^{n} \lambda(\vec{k}) \, \Delta t_i \tag{8.14}$$

or finally

$$P(t) = \exp \left(- \int_0^t \lambda(\vec{k}) \, dt'\right) \tag{8.15}$$

The probability density of an electron drifting for a time t and then suffering a collision is

$$p(t) = \lambda(\vec{k}) \, \exp \left(- \int_0^t \lambda(\vec{k}) \, dt'\right) \tag{8.16}$$

Using equation (8.3) which maps the probability density $p(t)$ to a uniformly distributed random number r we obtain

$$r = 1 - \exp \left(- \int_0^t \lambda(\vec{k}) \, dt'\right) \tag{8.17}$$

Mathematically it is possible to invert equation (8.17) and express t as a function of the random number r. In general it is complicated to perform such an inversion since an integral equation needs to be solved for each scattering event. The difficulty is not fundamental but lies in the numerical evaluation of the integrals. Rees [20] has devised a very simple method to overcome this difficulty. He introduced a new fictitious "self-scattering" such that the total scattering probability, including this self-scattering, is constant and equal to a certain constant Γ .

$$\Gamma = \lambda(\vec{k}) = \lambda_R(\vec{k}) + \lambda_V(\vec{k}) \tag{8.18}$$

where $\lambda_R(\vec{k})$ is the total real scattering rate and $\lambda_V(\vec{k})$ the total virtual or self-scattering rate. If the carrier undergoes such a self-scattering, its state $\vec{k}'$ after the collision is taken to be equal to its state k before the collision so that, in practice, the electron path continues unperturbed as if no scattering at all had occurred. Generally it is enough that Γ is larger than the maximum of $\lambda(\vec{k})$. Here Γ is taken as equal to $\sum\limits_{n=1}^{N} \lambda_n(E_{max})$ where the λ_n were defined in equation (8.9).

If $\lambda(\vec{k})$ is replaced by Γ in equation (8.17), then

$$r = 1 - \exp(-\Gamma t) \tag{8.19}$$

or

$$1 - r = \exp(-\Gamma t) \tag{8.20}$$

and

$$t = -\frac{1}{\Gamma} \ln(1 - r) \tag{8.21}$$

However, since r is evenly distributed between 0 and 1, so also is (1 - r), and in practice the following expression is used:

$$t = -\frac{1}{\Gamma} \ln(r) \tag{8.22}$$

The time given by equation 8.22 is not usually the flight time between real scattering processes, but is more likely to be the time between one virtual scattering process and another. The computer time "wasted" in taking care of self-scattering events is more than compensated for by

the simplification of the calculation of the free-flight time duration. The free flight must be terminated by a real scattering event. A further random number is then used to select a mechanism among all n different possible scattering mechanisms. This random number r is compared to the partial sums $\sum_{n=1}^{i} \lambda_n(k)$ normalized by Γ , where i varies from 1 to N the total number of scattering mechanisms considered in the model. If r is smaller than $\frac{1}{\Gamma} \sum_{n=1}^{i} \lambda_n(k)$, then the ith scattering mechanism is selected. If r is greater than the total scattering rate $\frac{1}{\Gamma} \sum_{n=1}^{N} \lambda_n(\vec{k})$, then a self-scattering or virtual scattering is chosen. This scattering process selection is described in Figure 8.4. In fact the method is exactly similar to that described earlier by equation (8.3). Instead of a continuous probability distribution function, we have here discrete events which are described in terms of sum of δ functions. The integral should be replaced by a discrete sum and the equality by a inequality sign.

8.2.e Choice of the State after Scattering

Once a type of scattering is selected to end a free-flight a new state $\vec{k}$ must be chosen. If the free flight ended with a virtual scattering, the state must remain the same before and after that virtual scattering. One the other hand, if a real scattering occurred, then the state $\vec{k}$ must be generated stochastically according to the differential cross section of that particular mechanism [18]. Especially different techniques are used to choose the post scattering angles for randomizing and non-randomizing mechanisms. The scattering involving acoustical phonons is randomizing while those involving polar optical phonons are not. These techniques will be described in more detail in section 8.3 when the Monte Carlo method is applied to calculate transport coefficients of a particular semiconductor material: GaAs.
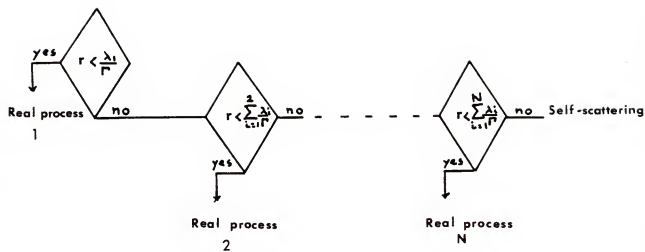
Figure 8.4: Scattering channel selection with N real scattering processes

8.2.f Collection of Results

The data collected at each free flight will form the base for the determination of the quantity of interest.

We obtain the average value of a quantity $A[k(t)]$ (e.g., the drift velocity, the mean energy, and so on) during a single history of duration T as

$$<A>_T = \frac{1}{T} \int_0^T A[k(t)]dt \qquad (8.23)$$

or

$$<A>_T = \frac{1}{T} \sum_i \int_0^{t_i} A[k(t)]dt \qquad (8.24)$$

where the total flight duration time T has been split into free flights of duration t_i. When a steady state quantity is computed, T should be taken sufficiently long enough so that $<A>_T$ in equation (8.24) represents the ensemble average of the quantity according to the ergodic theorem.

8.3 Application to Bulk GaAs Semiconductor

The energy-momentum band structure ($E(k)$ versus $\pm k$) of the GaAs material is shown in Figure 8.5. There is one central valley, with a small radius of curvature, where electrons have a low effective mass equal to 0.067 m_0, and there is a shallow satellite valley at the equivalent (100) Brillouin Zone Edges. By symmetry, however, identical sattelite valleys are located at the (010) and (001) edges as well. The valence band is well separated from the conduction band so the transport of holes is not considered.

For every type of scattering mechanism, the post scattering energy E(k') is calculated such that the energy conservation law is observed. In case of scatterings where acoustic phonons are involved, the process is assumed to be elastic with $E(k) = E(k')$.

The list of scattering processes considered in the work is given in Table 8.1 with their respective transition rate $S_n(k,k')$, total scattering rate $\lambda_n(k)$ $\lambda_n(E)$ and the energy conservation law for each type of scattering mechanism. The material parameters are given in Table 8.2.

8.3.a Angle Selections

As mentioned in section 8.2.e the state of the electron after a scattering process depends on the type of process involved. For the case of acoustic and intervalley processes, the transition probability S_n (k,k') (as listed in Table 8.1) does not depend upon the angle between k and k' so that all wave vectors that satisfy the appropriate law of conservation of energy are equally probable.

If the final momentum state k' makes an angle θ with the k_z-axis direction, then the probability density $p(\theta)$ is proportional to the number of states on the circumference of a circle of radius

$$|k'| \sin \theta = \frac{1}{\hbar} (2m^* E')^{1/2} \sin \theta \qquad (8.25)$$

where E' is the energy of the electron after scattering. This is sketched in Figure 8.6.

We assume that

$$p(\theta) = A \sin \theta \qquad (8.26)$$

The normalization requires that $A = 1/2$.
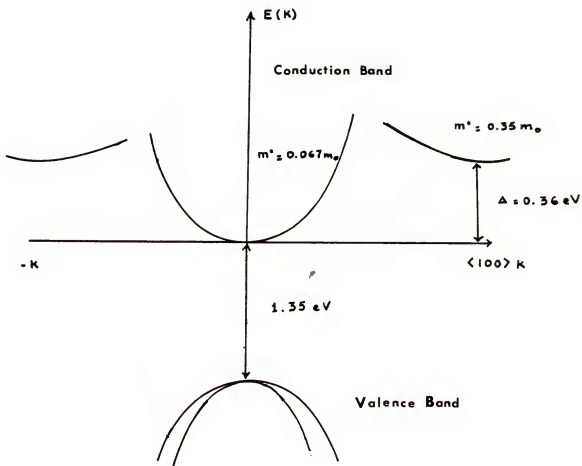
Figure 8.5: Band structure of GaAs

Table 8.1: Scattering mechanisms in GaAs from Boardman [19]

Scattering Mechanism	Transition Rate $(h/2\pi)S(K,K')$	Total Scattering Rate $\lambda(k) \equiv \lambda(E)$
Acoustic phonon for either absorption or emission (intervalley)	$$\frac{hD_a^2|\bar{K}-\bar{K}'|N_a\delta(A)}{(2\rho s)(2\pi)^3}$$ $$N_A \simeq \frac{k_BT}{hs|K-K'|}$$	$$\frac{(2m_c^*s)^{3/2}k_BTD_a^2E^{1/2}}{4\pi\rho\,s^2h^4}$$ absorption or emission $A = E'-E = 0$
Polar optical phonon (intravalley)	$$\frac{2\pi e^2 h\omega_o}{|K-K'|^2}\left(\frac{1}{\varepsilon_\infty}-\frac{1}{\varepsilon_0}\right)\frac{X}{4\pi\varepsilon_o(2\pi)^3}$$ $X = N_o\delta(A_a)$ absorption $= (N_o+1)\delta(Ae)$ emission $N_o = [\exp(h\omega_o/R_BT)-1]^{-1}$	$$\frac{\gamma_p^2 m^{*\,1/2}\omega_o}{\sqrt{2h}(4\pi\varepsilon)^2 E^{1/2}}\left(\frac{1}{\varepsilon_\infty}-\frac{1}{\varepsilon_0}\right)\ln\left|\frac{E^{1/2}+E'^{1/2}}{E^{1/2}-E'^{1/2}}\right|$$ $Y = N_o$ absorption $= (N_o+1)$ emission $A_{a,e} = E'-E \pm h\omega_o = 0$
Equivalent intervalley (satellite-satellite)	$$\frac{(z-1)hD_e^2 X}{(2\pi)^3(2\rho\omega_e)}$$ $X = N_e\delta(A_a)$ absorption $= \delta(A_e)$ emission (N_e+1) $N_e = [\exp(h\omega_e/k_BT)-1]^{-1}$	$$\frac{(z-1)m_s^{3/2}D_e^2E^{1/2}Y}{\sqrt{2}\,\pi\rho\omega_e h^3}$$ $Y = N_e$ absorption $= $ emission (N_e+1) $A_{a,e} = E'-E \pm h\omega_e = 0$
Non-equivalent intervalley a) central → satellite	$$\frac{3hD_n^2X}{2\rho\omega_n(2\pi)^3}$$ $X = N_n\delta(A_a)$ absorption $= (N_n+1)\delta(A_e)$ emission	$$\frac{3m_s^{3/2}D_n^2E^{1/2}Y}{\sqrt{2}\pi\rho\omega_n h^3}$$ $Y = N_n$ absorption $= (N_n+1)$ emission $A_{a,e} = E'-E+\Delta \pm h\omega_n = 0$
b) satellite → central	$$\frac{hD_n^2X}{2\rho\omega_n(2\pi)^3}$$ $X = N_n\delta(A_a)$ absorption $(N_n+1)\delta(A_e)$ emission $N_n = [\exp(h\omega_n/k_BT)-1]^{-1}$	$$\frac{m_c^{3/2}D_n^2E^{1/2}Y}{\sqrt{2}\pi\rho\omega_n h^3}$$ $Y = N_n$ absorption (N_n+1) emission $A_{a,e} = E'-E-\Delta \pm h\omega_n = 0$

Table 8.2: Data for GaAs from Boardman [19]

Density, ρ	5.37 g/cm^3
Velocity of sound, s	5.22×10^5 cm/s
High frequency dielectric constant, ϵ_∞	10.82
Static dielectric constant, ϵ_0	12.53
Polar optical phonon frequency, ω_0	5.37×10^{13} rad.s^{-1}
Equivalent intervalley phonon frequency, ω_e	4.54×10^{13} rad.s^{-1}
Non-equivalent intervalley phonon frequency, ω_n	4.54×10^{13} rad.s^{-1}
Acoustic deformation potential in central and satellite valleys, D_a	7eV
Equivalent intervalley deformation potential, D_e	10^9eV/cm
Non-equivalent intervalley deformation potential, D_n	10^9eV/cm
Central valley effective mass, $m_c^\star$	0.067 m_0
Satellite valley effective mass, $m_s^\star$	0.35 m_0
Valley separation, Δ	0.36 ρV

Mapped with a uniform random distribution, sin θ can be generated using the following relations:

$$r = \int_0^\theta p(\theta') \, d\theta' \qquad (8.27)$$

$$r = 1/2 \, (1 - \cos \theta) \qquad (8.28)$$

the new state k' is therefore

$$\vec{k}' = (|k'| \sin \theta, \, |k'| \cos \theta) \qquad (8.29)$$

The situation for polar optical phonon scattering is completely different, since the transition rate $S_n(k,k')$ as shown in Table 8.1 depends upon the angle between k and k' through the factor $|\vec{k} - \vec{k}'|^{-2}$.

It is necessary to consider first the angle β between k and k' using k as reference as shown Figure 8.7.a.

The probability density p(β), as in the previous mechanisms is proportional to sin β and also must be weighted by the factor $|k-k'|^{-2}$.

$$p(\beta) = \frac{A \sin \beta}{|k - k'|^2} \qquad (8.30)$$

The factor $|k - k'|^2$ can be expressed in terms of E and E', the energies of the states k and k' respectively and β as follows:

$$|k - k'|^2 = \frac{2m^\star}{\hbar^2} \, (E + E' - 2(EE')^{1/2} \cos \beta) \qquad (8.31)$$

then
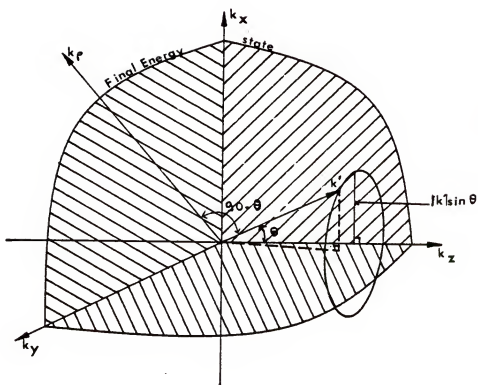
Figure 8.6: Angle selection for acoustic and intervalley process

Figure 8.7: Angle selection for polar optical
phonon process

$$p(\beta) = \frac{\beta \sin \beta}{E + E' - 2(EE')^{1/2} \cos \beta} \qquad (8.32)$$

where $B = \frac{A \hbar^2}{2m^*}$

Let $f = \frac{2(EE')^{1/2}}{(E^{1/2} - E'^{1/2})^2}$, $x = \cos \beta$

Then $\cos \beta$ can be chosen by a random number r as

$$r = \frac{\int_{\cos \beta}^{1} \frac{dx}{(1 + f - fx)}}{\int_{-1}^{1} \frac{dx}{(1 + f - fx)}} \qquad (8.33)$$

or carrying out the integrals

$$r = \frac{\ln (1 + f - f \cos \beta)}{\ln (1 + 2f)} \qquad (8.34)$$

Thus

$$\cos \beta = \frac{1 + f + (1 + 2f)^r}{f} \qquad (8.35)$$

As is shown in Figure 8.7.a, all possible positions of $\vec{k}'$ are generators of a cone about $\vec{k}$, of semi-angle β. The azimuthal angle ϕ shown in Figure 8.7.a can be selected with a random number such that

$$\phi = 2\pi r \qquad (8.36)$$

$r \in [0, 1]$

The coordinates of $\vec{k}'$ in the $k_z - k_\rho$ plane is then

$$k'_z = |k'| \cos \gamma \qquad (8.37)$$

$$k'_\rho = |k'| \sin \gamma$$

where γ is the angle between $\vec{k}'$ and $\vec{F}$ as shown in Figure 8.7.b. The angle γ is related to ϕ and β in the following way:

$$\cos \gamma = \cos \beta \cos \psi + \sin \beta \sin \psi \cos \phi \qquad (8.38)$$

where ψ is the angle between $\vec{k}$ and $\vec{F}$. The angle ψ can be determined by $\cos \psi = k_z/|k|$ where k_z is known at the end of the free flight and $|k| = (2m*E)^{1/2}/\hbar$. .

For the different types of scattering considered here then, the post-scattering wave vector $\vec{k}'$ is completely determined. The wave vector $\vec{k}'$ will be the initial value for the next free flight.

8.3.b Drift Velocity and Diffusion Coefficient

The velocity of an electron can be expressed as

$$\vec{v} = \frac{\hbar \vec{k}}{m*} \qquad (8.39)$$

so the mean velocity is

$$\langle \vec{v} \rangle = \hbar/m* \frac{\int_{all} \vec{k} \, p \, (\vec{k}) \, \vec{k} \, d \, \vec{k}}{\int_{all} \vec{k} \, p \, (\vec{k}) \, d \, \vec{k}} \qquad (8.40)$$

However, in the k_z direction the motion is uniform since the electron is under a constant electric field $\vec{F}$, then the distribution $p(k_z) = 1$ and if the integral is split into a sum of integrals over a free flight equation (8.40) becomes

$$\langle v \rangle = \frac{\hbar/m^* \quad \sum\limits_{\text{free flights}} \int\limits_{k_{z_i}}^{k_{z_f}} k_z \, d k_z}{\sum \int\limits_{k_{z_i}}^{k_{z_f}} d k_z} \tag{8.41}$$

This represents the mean drift velocity in the z-direction. Carrying out the integrals, we obtain;

$$v_{\text{drift}} = \frac{\hbar}{2m^*} \frac{\sum (k_{z_f}^2 - k_{z_i}^2)}{D} \tag{8.42}$$

where $D = \sum \int\limits_{k_{z_i}}^{k_{z_f}} d k_z$

This is very convenient to use because k_{z_f}, k_{z_i} are z-components of the final and initial $\vec{k}$ vector for a free flight. They are known once the energy is known and the type of scattering mechanism is selected. The computation of v is then a matter of recording these values. The drift velocity as a function of electric field obtained from this method for a bulk GaAs semiconductor is shown in Figure 8.8.

The longitudinal diffusion can be obtained from Einstein's equation

$$\text{var } z = 2 D t \tag{8.43}$$

where z is the displacement and D the diffusion coefficient.

It is therefore expected that if the motion of a single electron from an initial position (0,0,0) is observed over a sampling time T and a large number of samples are taken, then the displacements for the different samples should have the same variance.

To make good use of the simulation of the drift velocity, equation 8.43 can be rewritten for a fixed T as

$$T \text{ var } v_z = 2 D \qquad (8.44)$$

or

$$D = 0.5 \; T \; (<v_z^2> - <v_z>^2) \qquad (8.45)$$

where v_z is the average drift velocity in the z direction and T sampling time.

The simulation of the drift velocity can be performed in two ways: either the number of real scattering events is fixed or the total sampling time is fixed. The latter method is used to calculate the diffusion coefficient, since to be valid, equation (8.43) requires that T is constant. The diffusion coefficient D as a function of the electric fields is plotted in Figure 8.9 for a bulk GaAs semiconductor.

The programs used to simulate v(E) and D(E) are listed in Appendix 1.

The drift velocity and the diffusion coefficient obtained from this Monte Carlo simulation are used to calculate the high frequency noise. This will be described in Chapter IX.
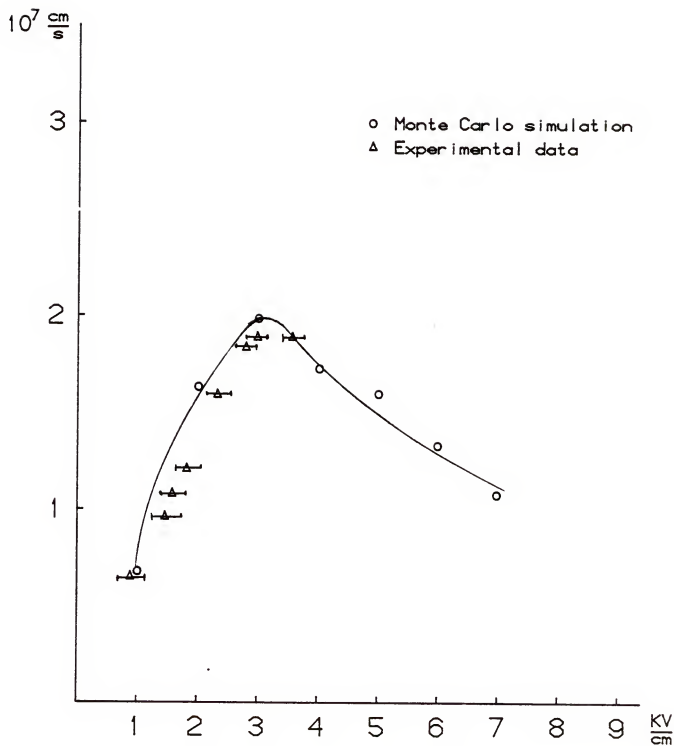
Figure 8.8: Electron drift velocity as a function
of electric field
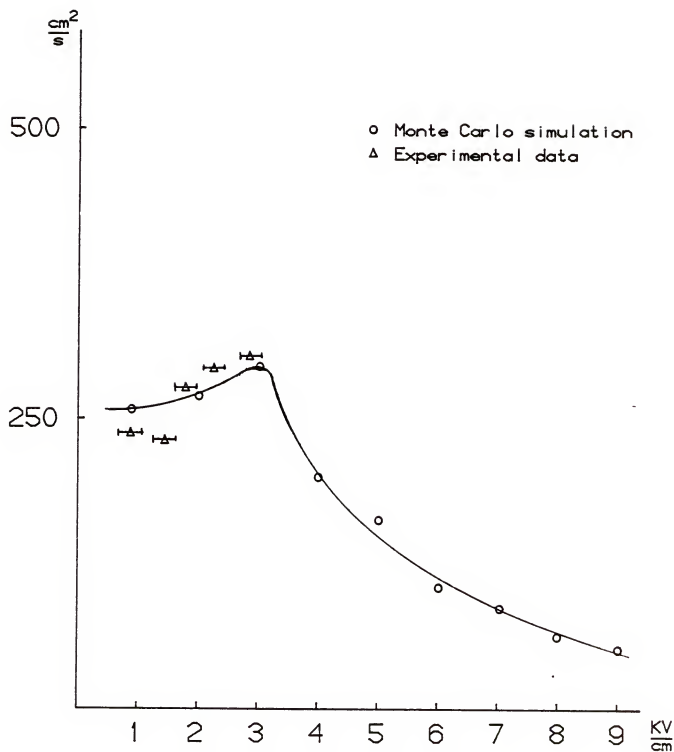
Figure 8.9: Electron diffusion coefficient as a function of the electric field

CHAPTER IX
DISCUSSIONS

In Chapter VII, the experimental results of the high frequency noise measurements were presented. In Chapter VIII the electron drift velocity and the electron diffusion coefficient were computed using the Monte Carlo simulation method. One would like to compare the experimental data with the theoretical calculations. That will be the subject of this chapter.

Using Poisson's equation and the current equation, neglecting the displacement current and the diffusion current, one can express the length of the device L and the applied voltage at the anode V_0 as a function of the applied field, in an integral form;

$$V_0 = \frac{\varepsilon A}{I_0} \int_0^{E_L} \frac{E^2 \mu(E)\,dE}{(1-q\frac{AN_D E\mu(E)}{I_0})} \qquad (9.1)$$

$$L = \frac{\varepsilon A}{I_0} \int_0^{E_L} \frac{E\mu(E)\,dE}{(1-q\frac{AN_D E\mu(E)}{I_0})} \qquad (9.2)$$

where V_0 = bias voltage, I_0 = DC current, A = cross-sectional area, L = contact spacing, E_L = electric field strength at the anode, N_D = concentration of fully ionized donors, and ε = permittivity. In these

two equations the field dependence of the electron mobility is taken
into account. Moreover, Gisolf and Zijlstra [21] derived an integral
form of the noise spectral density, taking space charge injection and
carrier heating into account;

$$S_{\Delta V}(f) = \frac{4\varepsilon qA}{I_o^2} \int_o^{E_L} \frac{D(E)(E_L-E)^2 dE}{(1-q\frac{AN_D\mu(E)E}{I_o})^3}$$ (9.3)

where $D(E)$ is the electron diffusion coefficient. Equation (9.3)
together with equations (9.1) and (9.2) forms a system of integral
equations with three unknowns, namely E_L, $\mu(E)$, and $D(E)$. This system
is difficult to solve analytically. Numerical techniques are required
to circumvent such difficulty. This will be discussed in the following
section.

9.1. Numerical Decomposition of the Current-Voltage Characteristic and the Noise Spectrum Density

Bosman [22] developed a method to solve numerically equations
(9.1), (9.2), and (9.3). He considered equally spaced bias voltage
values V_{o_i} (i = 1...N). For each V_{o_i}, there is a one to one
correspondence between the current value I_{o_i}, the noise spectral density
$S\Delta V_{o_i}$, and the electric field strength E_{L_i}. To every E_{L_i} corresponds a
value of $\mu(E)$ and $D(E)$.

He assumed that between two consecutive values of E_{L_i}, the electron
mobility and the electron diffusion coefficient are constant;

$$D(E) = D_i \text{ and } (E) = \mu_i$$ (9.4)

for $\quad E_{L_i} \leqslant E \leqslant E_{L_{i+1}}$

Using the assumptions stated in equation (9.4), equations (9.1), (9.2), and (9.3) can be rewritten as

$$V_{O_i} = \frac{\varepsilon A}{I_{O_i}} \sum_{s=1}^{i} \int_{E_{L_{s-1}}}^{E_{L_s}} \frac{\mu_s E^2 dE}{(1 = q \frac{A N_D \mu_s E}{I_{O_i}})} \tag{9.5}$$

$$L = \frac{\varepsilon A}{I_{O_i}} \sum_{s=1}^{i} \int_{E_{L_{s-1}}}^{E_{L_s}} \frac{\mu_s E dE}{(1 - q \frac{A N_D \mu_s E}{I_{O_i}})} \tag{9.6}$$

$$S_{\Delta V_i}(f) = \frac{4 \varepsilon q A}{I_{O_i}^2} \sum_{s=1}^{i} \int_{E_{L_{s-1}}}^{E_{L_s}} \frac{D_s (E_{L_i} - E)^2 dE}{(1 - q \frac{A N_D \mu_s E}{I_{O_i}})^3} \tag{9.7}$$

The integral equations are now transformed into a system of three non-linear equations with three unknowns, E_{L_i}, μ_i, and D_i. For a given i, equations (9.5) and (9.6) are solved first to obtain μ_i and E_{L_i}, then these values are substituted in equation (9.7) to calculate D_i. All the integrals in equations (9.5), (9.6), and (9.7) can be evaluated analytically. This process is done iteratively to give μ_i, D_i, and E_{L_i} in ascending order of i. The details of these calculations are given in Appendix 2.

The accuracy of the results depends strongly on the magnitude of the interval $[E_{L_i}, E_{L_{i+1}}]$. Another difficulty in the calculations is

the fact that the numerical solutions can be unstable due to the presence of a pole in the integrand of the integrals in equation (9.5), (9.6), and (9.7).

The diffusion coefficient and the electron drift velocity obtained from this decomposition are plotted along with the values obtained by Monte Carlo simulation in Chapter VIII. A difficulty one might encounter in the measurement of high field properties of GaAs is the possible occurrence of traveling domains. These domains would make the electric field inside the device dependent on position and time. However, according to Kroemer [23], these dipole domains are formed only when $N_D L$ exceeds 2×10^{12} cm^{-2}. This is not the case here where N_D is 2×10^{15} cm^{-3} and L is 1.1µm. No traveling dipole effects were observed during the measurements.

In conclusion of these high frequency noise measurements we found that the noise of a 1.1µm n-type GaAs device at high bias voltages can be explained in terms of the hot electron properties of the mobility and diffusion coefficient if the field dependence of these parameters is taken into account properly.

In Chapter X, we will present the conclusion of the overall work and suggest some numerical simulations and experimental work to pursue in these very short structures.

CHAPTER X
CONCLUSION AND RECOMMENDATIONS FOR FUTURE WORK

10.1 1/f Noise and Ballistic Transport

10.1.a Numerical Simulation

One problem encountered in Chapter V for the calculation of α_H was the determination of the total number carriers N_{eff}. As we should understand, N_{eff} is the total number of carriers which suffer scatterings. For short devices, as Hesto [24] mentioned, an important fraction of the electrons does not suffer any collision at all. For a given electric field, this fraction of ballistic electrons can be obtained through Monte Carlo simulation. Hesto showed at 77 K, this fraction is still important for distances as long as 0.35 μm. This consideration would improve greatly the computation of N_{eff} mentioned in Chapter V. Such a Monte Carlo simulation may give information about the current due to ballistic and non-ballistic electrons. Device simulations initiated by Tehrani [14] should be further pursued taking into account these ballistic effects. The idea is as follows:

The Monte Carlo simulation should give th electron distribution at each time, then the electric field is calculated by solving Poisson's equation.

10.1.b Other Experiments on Short Structures

As stated previously in section 10.1.a, for low temperature and if the thickness of the low doped region is sufficiently small

(L ≤ 0.5 m), an important fraction of the electron population can flow through the device having a small number of interactions or even no interaction at all with the polar optical phonons and then can reach the anode with high kinetic energy. It has also been shown in Chapter II that the current-voltage characteristic of a device is not sufficient to determine whether the transport is ballistic or not.

An experiment which allows separation of groups of electrons according to their kinetic energy is probably interesting.

Hesto et al. [25] proposed the following experiment. They added a Schottky contact at the end of the regular $N^+ N^- N^+$ device in a way that it opposes its variable potential barrier ϕ_B to the electron energy. The device is described in Figure 10.1.

Let respectively V_{BE} and V_{CB} be the $N^+ N^- N^+$ and the Schottky bias voltages. The electrons having a ballistic flight through the N^- region have a fast transit through the N^+ region and then move against the retarding electric field of the Schottky barrier. By this way, only those having their kinetic energy at the end of the N region higher than the Schottky barrier ϕ_B reach the anode. By varying V_{CB} one controls the height of this Schottky barrier. The result would result in good separation of these groups of electrons.

10.2 High Frequency Noise Measurements

The same measurements as described in Chapter VI and VII should be repeated for the shorter devices. However, the simulation of $v(E)$ and $D(E)$ should be changed. The method used in Chapter VIII for Monte Carlo simulation is not valid anymore in the case of short devices. The ergodicity theorem does not apply in this case. Instead of time average, we have to perform an ensemble average. The average value is
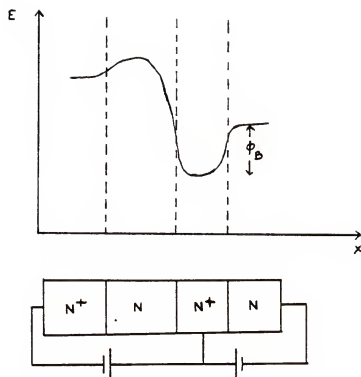
Figure 10.1: $N^+ N N^+$ Schottky barrier device

performed at a preselected time so that we would have the average velocity, the diffusion coefficient as a function of time.

Taking a Fourier transform of the diffusion equation Jacoboni and Reggiani [18] showed that the diffusion coefficient can be calculated through Monte Carlo simulation as a function of frequency and the reciprocal of the distance. This approach is necessary if one wants to calculate the diffusion coefficient at short times and short distances.

APPENDIX 1
MONTE CARLO SIMULATION PROGRAM

```
C      COMPUTER SIMULATION OF THE DRIFT VELOCITY,MEAN
C      ENERGY AND DISTRIBUTION FUNCTION OF HOT
C      ELECTRON
       DOUBLE PRECISION*6 KB ,KRHO,KZF ,KII,KT ,M
      1,NO,NE,NI,KITOT,V4VG,V2AVG,V3AVG,V4AVG,DIF
      1, IF4,FT,TF,VI,TTOT
       DOUBLE PRECISION*6  F(10),GAMMA(2),EF(10),SCATT(10)
      1,DK(2),L(10)
       INTEGER*6 NF,VV,VR,TT,V,SR,SS,K,GMAX,NCIF
C
C      FUNDAMENTAL CONSTANTS
C
       H=1.05459
       E=1.60219
       C=4.303213
       KB=1.38062
       M=9.109136
C
C      DATA ON MATERIAL GAAS
C
       WRITE(6,41)
41     FORMAT(10X,'MATERAL DENSITY(GM.CM-3)')
       READ(11,689)RHE
       WRITE(6,42)
42     FORMAT(10X,'VELOCITY OF SOUND(10**5CM/S-1)')
       READ(11,689)S
       WRITE(6,43)
43     FORMAT(10X,'HIGH FREQUENCY DIELECTRIC CONSTANT')
       READ(11,689)R1
       WRITE(6,44)
44     FORMAT(10X,'LOW FREQUENCY DIELECTRIC CONSTANT')
       READ(11,689)R2
       WRITE(6,1)
1      FORMAT(10X,'OPTICAL PHONON FREQUENCY(10**13RAO.S-1)')
       READ(11,689)WO
       WRITE(6,2)
2      FORMAT(10X,'EQU. INTERVALLEY PHONON FREQ.')
       READ(11,689)WE
       WRITE(6,3)
3      FORMAT(10X,'INTERVALLEY PHONON FREQUENCY')
       READ(11,689)WI
       WRITE(6,4)
4      FORMAT(10X,'ACOUSTIC DEFORMATION POTENTAL(EV)')
       READ(11,689)THA
       WRITE(6,5)
5      FORMAT(10X,'EQU.INTERVALLEY DEF.POTENTIAL(EV)')
       READ(11,689)THE
       WRITE(6,6)
6      FORMAT(10X,'INTERVALLEY DEF.POTENTIAL')
       READ(11,689)THI
       WRITE(6,7)
7      FORMAT(10X,'VALLEY SEPARATION')
       READ(11,689)D
       WRITE(6,8)
8      FORMAT(10X,'CENTRAL VALLEY EFFECTIVE MASS')
```

```
      READ(11,689)EM1
      WRITE(6,9)
9     FORMAT(10X,'SATELLITE VALLEY EFF.MASS')
      READ(11,689)EM2
689   FORMAT(E10.4)
C
C
C     FINAL DATA INPUT
C
40    WRITE(5,10)
10    FORMAT(10X,'TEMPERATURE(KELVIN)')
      READ(11,531) T
531   FORMAT(E10.4)
      WRITE(5,21)
21    FORMAT(10X,'MAXIMUM ENERGY(EV)')
      READ(11,532) EMAX
532   FORMAT(E10.4)
      WRITE(5,11)
11    FORMAT(10X,'NUMBER OFAVERAGES')
18    READ(11,533) NDIF
533   FORMAT(I5)
      IF(THI.NE.0.0) GO TO 750
      IF(NDIF.LE.3000) GO TO 16
      WRITE(5,710)
710   FORMAT(10X,'MAXIMUM COLLISIONS IN ONE VALLEY=3000')
      GO TO 13
750   IF(NDIF.LE.20000) GO TO 16
      WRITE(5,17)
17    FORMAT(10X,'MAXIMUM COLLISIONS IN TWO VALLEYS=2000')
      GO TO 18
16    WRITE(5,12)
12    FORMAT(10X,'NUMBER OF ELECTRIC FIELDS')
      READ(11,534) NF
534   FORMAT(I2)
      DO 30 I=1,NF
      WRITE(5,13) I
13    FORMAT(10X,'FIELD',I2)
      READ(11,535) F(I)
535   FORMAT(E12.4)
30    CONTINUE
      WRITE(5,23)
23    FORMAT(10X,'VALLEY FOR DISTRIBUTION FUNCTION :1 OR 2')
      READ(11,536) VV
536   FORMAT(I2)
      WRITE(5,22)
22    FORMAT(10X,'DISTANCE FROM KZ AXIS OF DISTRIBUTION :1 TO 21')
      READ(11,537) VR
537   FORMAT(I2)
      READ(11,532) DL
C
C     CALCULATE PHONON FREQUENCIES AND OCCUPATION RATIOS
C
      HWO=H*WO/(E*100.0)
      HWI=H*WI/(E*100.0)
      HWE=H*WE/(E*100.0)
```

```
      IF(WO.NE.0.0) GO TO 909
      NO=0.0
      GO TO 908
909   NO=1/(EXP((WO*76.385)/T)-1)
908   NI=1/(EXP((WI*76.385)/T)-1)
      NE1=1/(EXP((WE*76.385)/T)-1)
C
C         CONSTANTS FOR SCATTERING RATES
C
      C1=1.0E+12*C*C*SQRT(M)*WO*(1/R1-1/R2)*(NO+1)/(1.4142*H*SQRT(E))
      C2=C1*NO/(NO+1)
      C3=1.0E+10*(2*M)**1.5*KB*T*THA*THA*E*E*SQRT(E)/(4.0*3.142*RHE
     1*S*S*H*H*H*H)
      C4=2.0E+14*M**1.5*THE*THE*E*E*(NE+1)*SQRT(E)
     1/(1.4142*3.142*RHE*WE*H*H*H*H)
      C5=C4*NE/(NE+1)
      C6=1.0E+14*(EM1*M)**1.5*THI*THI*E*E*(NI+1)*SQRT(E)/(1.4142*3.142
     1*RHE*WI*H*H*H*H)
      C7=3.0E+14*(EM2*M)**1.5*THI*THI*E*E*(NI+1)*SQRT(E)/(1.4142
     1*3.142*RHE*WI*H*H*H*H)
      C8=C7*NI/(NI+1)
      C9=C6*NI/(NI+1)
C
C         CALCULATE K SPACE MESH ELEMENT FOR BOH VALLEYS
C
      DK(1)=1.0E+7*SQRT(2*EM1*M*EMAX*E)/(H*20.0)
      DK(2)=1.0E+7*SQRT(2*EM2*M*EMAX*E)/(H*20.0)
C
C         CALCULATE VALUES OF KZ AT CENTRE OF EACH MESH ELEMENT
C         IN CHOSEN VALLEY AND WRITE TO FILE
C
      KZI=-DK(VV)*9.5
      DO 805 LL=1,20
      WRITE(5,807) KZI
807   FORMAT(E12.4)
      KZI=KZI+DK(VV)
805   CONTINUE
C         SET PARAMETERS FOR CENTRAL VALLEY,THEN CALCULATE THE
C         TOTAL SCATTERING RATE FOR REAL PROCESSES(R) FOR A NUMBER
C         OF ENERGIES UP TO THE MESH SIZE.STORE MAXIMUM VALUE OF R
C         IN GAMMA(1) TO CALCULATE PSEUDO (SELF) SCATTERING RATE.
C         TT=1 ENABLES PROGRAM TO RETURN TO LABEL 40
C
      TT=1
      EM=EM1
      V=1
31    GAMMA(V)=0.0
      EI=0.0
      J=1
35    EI=EI+EMAX/20.0
      GO TO 100
40    R=0.0
      DO 50 I=1,10
      R=R+L(I)
50    CONTINUE
```

```
        IF(R.GT.GAMMA(V)) GAMMA(V)=R
        J=J+1
        IF(J.NE.21) GO TO 35
C
C         SET PARAMETERS FOR SATELLITE VALLEY AND REPEAT PROCESS TO
C         OBTAIN GAMMA(2).
C
        IF(V.EQ.2) GO TO 71
        EM=EM2
        V=2
        GO TO 31
71      WRITE(5,75) GAMMA(1),GAMMA(2)
        WRITE(7,75) GAMMA(1),GAMMA(2)
75      FORMAT(10X,'GAMMA(1)=',E10.4,'GAMMA(2)=',E10.4)
        WRITE(5,72) T,NDIF,EMAX
        WRITE(7,72) T,NDIF,EMAX
72      FORMAT(10X,'TEMP=',E10.4,5X,'REALCLSNS=',I4,5X,'MAXENERGY='
       1,E10.4)
C
C         SET MESH REGISTERS TO ZERO AND PLACE ELECTRON AT
C         STARTING POINT IN MESH.TT=0 FOR ITERATIVE PROCESS
C
        TT=0
        J=1
        TTOT=0.0
        OTOT=0.0
        NN=0
        VAVG=0.0
        V2AVG=0.0
        DIF=0.0
        V3AVG=0.0
        V4AVG=0.0
        DIF4=0.0
        CHECK=0.0
        TF=4.0E-10
        FT=TF
        IDIF=0
        ETOT=0.0
        KZTOT=0.0
        NPRINT=0
30      V=1
        EM=EM1
        KRHO=0.0
        SR=0
        SS=0
        GMAX=0
C
C         IF NO. OF REAL PROCESSES EQUALS CHOSEN VALUES
C         END ITERATION AND GO TO FINAL CALCULATION.
C
C         CALL RANDOM NUMBER(NOT=C) AND CALCULATE TIME OF
C         FLIGHT UNDER ELECTRIC FIELD AND NEW POSITION OF
C         ELECTRON K SPACE
C
```

```
37      R=RANU(0.0,1.0)
        KZF=(10.0/H)*SQRT(20.0*K9*T*EM*M*(-ALOG(R)))
90      IF(TTOT.GT.FT) GO TO 470
        R=RANU(0.0,1.0)
        IF(R.EQ.0.0) P=1.0E-20
        TIME=-ALOG(R)/GAMMA(V)
        KZI=KZF*(TIME*E*F(J)*1.0E+18)/H
        KT=SQRT(KRHO*KRHO+KZI*KZI)
        EI=H*H*KT*KT*1.0E-14/(E*2*EM*M)
C
C       IF ELECTRON LEAVES MESH PLACE IT ON EDGE OF MESH AND
C       REGISTER OCCURRENCE IN COUNTER GMAX
C
        IF(EI.LE.EMAX) GO TO 95
        GMAX=GMAX+1
        EI=EMAX
        KT=1.0E+7*SQRT(2*EM*M*EMAX*E)/H
        IF(KZI.GT.0.0) GO TO 94
        KZI=-SQRT(ABS(KT*KT-KRHO*KRHO))
        GO TO 95
94      KZI=SQRT(ABS(KT*KT-KRHO*KRHO))
C
C       STORE FLIGHT TIME IN TOTAL TIME REGISTER FOR APPROPRIATE
C       VALLEY,THEN REGISTER PASSAGE OF ELECTRON THROUGH ELEMENTS
C       OF K SPACE MESH
C
95      TTOT=TTOT+TIME
        IF(NN.NE.0) GO TO 96
        O=H*10.0*TIME*(KZI+KZF)/(2*EM*M)
        OTOT=OTOT+O
        IF(OTOT.LT.OL) GO TO 96
        TF=TTOT-TIME
        FT=TF
        NN=NN+1
96      KZTOT=KZTOT+ABS(KZI-KZF)
        ETOT=ETOT+(KZI*KZI+KZF*KZF)*10.0*H/(2*EM*M)
C
C       SUM TOTAL CHANGES IN K SPACE POSITION AND ENERGY SPACE POSITON
C       AND STORE IN KZTOT AND ETOT.SUM MEAN ENERGY CHANGE IN MNE.
C       SUM INDIVIDUAL VALUES FOR EACH VALLEY IN KZ(V) AND ET(V).
C
C
C       CHECK FOR ROUNDING ERRORS LEADING TO NEGATIVE ENERGY VALUES.
C       IF THIS OCCURS,PLACE ELECTRON AT STARTING POSITION.
C
        IF(EI.GT.0.0) GO TO 100
        KRHO=0.0
        KZF=1.0E+6
        EM=EM1
        V=1
        GO TO 90
C       CALCULATE FINAL ENERGY VALUE FOR EACH SCATTERING PROCESS
C
100     EF(1)=EI-HWO
```

```
      EF(2)=EI+HWO
      EF(3)=EI
      EF(4)=EI
      EF(5)=EI-HWE
      EF(6)=EI+HWE
      EF(7)=EI-HWI+D
      EF(8)=EI-HWI-D
      EF(9)=EI+HWI-D
      EF(10)=EI+HWI+D
C
C        SCATTERING RATES FOR REAL PROCESSES
C
      IF(EF(1).GT.0.0) GO TO 110
      L(1)=0.0
      GO TO 120
110   L(1)=C1*SQRT(EM)*ALOG(ABS((SQRT(EI)+SQRT(EF(1)))/(SQRT(EI)-
     1SQRT(EF(1)))))/SQRT(EI)
C
C      EMISSION OF OPTICAL PHONON
C
120   IF(EF(2).GT.0.0) GO TO 125
      L(2)=0.0
      GO TO 130
125   L(2)=C2*SQRT(EM)*ALOG(ABS((SQRT(EI)+SQRT(EF(2)))/(SQRT(EI)-
     1SQRT(EF(2)))))/SQRT(EI)
C
C      ABSORPTION OF OPTICAL PHONON
C
130   IF(EF(3).GT.0.0) GO TO 135
      L(3)=0.0
      GO TO 140
135   L(3)=C3*EM**1.5*SQRT(EF(3))
C
C      EMISSION OF ACOUSTIC PHONON
C
140   IF(EF(4).GT.0.0) GO TO 145
      L(4)=0.0
      GO TO 150
145   L(4)=L(3)
C
C      ABSORPTION OF ACOUSTIC PHONON
C
150   IF(EF(5).GT.0.0) GO TO 155
      L(5)=0.0
      GO TO 170
155   IF(V.EQ.2) GO TO 160
      L(5)=0.0
      GO TO 170
160   L(5)=C4*EM**1.5*SQRT(EF(5))
C
C        EMISSION OF EQUIVALENT INTERVALLEY PHONON
C
170   IF(EF(6).GT.0.0) GO TO 175
      L(6)=0.0
      GO TO 190
```

```
175   IF(V.EQ.2) GO TO 180
      L(6)=0.0
      GO TO 190
180   L(6)=C5*EM**1.5*SQRT(EF(6))
C
C        ABSORPTION OF EQUIVALENT INTERVALLEY PHONON
C
190   IF(EF(7).GT.0.0) GO TO 195
      L(7)=0.0
      GO TO 210
195   IF(V.EQ.2) GO TO 200
      L(7)=0.0
      GO TO 210
200   L(7)=C6*SQRT(EF(7))
C
C        EMISSION OF INTERVALLEY PHONON(SATELLITE TO CENTRAL)
C
210   IF(EF(8).GT.0.0) GO TO 215
      L(3)=0.0
      GO TO 230
215   IF(V.EQ.1) GO TO 220
      L(3)=0.0
      GO TO 230
220   L(3)=C7*SQRT(EF(3))
C
C        EMISSION OF INTERVALLEY PHONON(CENTRAL TO SATELLITE)
C
230   IF(EF(9).GT.0.0) GO TO 235
      L(9)=0.0
      GO TO 250
235   IF(V.EQ.1) GO TO 240
      L(9)=0.0
      GO TO 250
240   L(9)=C8*SQRT(EF(9))
C
C        ABSORPTION OF INTERVALLEY PHONON(CENTRAL TO SATELLITE)
C
250   IF(EF(10).GT.0.0) GO TO 255
      L(10)=0.0
      GO TO 270
255   IF(V.EQ.2) GO TO 260
      L(10)=0.0
      GO TO 270
260   L(10)=C9*SQRT(EF(10))
C
C        ABSORPTION OF INTERVALLEY PHONON(SATELLITE TO CENTRAL)
C
270   IF(TT.EQ.1) GO TO 40
C
C     CALCULATE SUM OF REAL PROCESS SCATTERING RATES
C
280   SCATT(1)=L(1)/GAMMA(V)
      DO 290 K=2,10
      SCATT(K)=SCATT(K-1)+L(K)/GAMMA(V)
290   CONTINUE
```

```
C
C        CALL RANDOM NUMBER.SELECT SCATTERING CHANNEL
C
        R=RANU(0.0,1.0)
        IF(R.LT.SCATT(1)) GO TO 300
        IF(R.LT.SCATT(2)) GO TO 310
        IF(R.LT.SCATT(3)) GO TO 320
        IF(R.LT.SCATT(4)) GO TO 330
        IF(R.LT.SCATT(5)) GO TO 340
        IF(R.LT.SCATT(6)) GO TO 350
        IF(R.LT.SCATT(7)) GO TO 360
        IF(R.LT.SCATT(8)) GO TO 370
        IF(R.LT.SCATT(9)) GO TO 380
        IF(R.LT.SCATT(10)) GO TO 390
        GO TO 400
C
C        SET ENERGY AFTER SCATTERING PROCESS
C
300     EFIN=EF(1)
        GO TO 420
310     EFIN=EF(2)
        GO TO 420
320     EFIN=EF(3)
        GO TO 410
330     EFIN=EF(4)
        GO TO 410
340     EFIN=EF(5)
        GO TO 410
350     EFIN=EF(6)
        GO TO 410
360     EFIN=EF(7)
        GO TO 430
370     EFIN=EF(8)
        GO TO 430
380     EFIN=EF(9)
        GO TO 430
390     EFIN=EF(10)
        GO TO 430
400     EFIN=EI
        GO TO 450
410     SR=SR+1
C
C        REGISTER REAL COLLISION.CALCULATE K SPACE POSITION AFTER
C        ACOUSTIC,INTERVALLEY OR EQUIVALENT INTERVALLEY PHONON SCATTERING
C
        R=RANU(0.0,1.0)
        KT=1.0E+7*SQRT(2*EM*M*EFIN*E)/H
        KZF=KT*(1-2*R)
        KRHO=KT*SQRT(4*R*(1-R))
        GO TO 450
420     SR=SR+1
C
C        REGISTER REAL COLLISION.CALCULATE K SPACE POSITION AFTER
C        OPTICAL PHONON SCATTERING
C
```

```
        R=RANU(0.0,1.0)
        U=RANU(0.0,1.0)
        PHI=2*3.142*R
        EX=2*SQRT(EFIN*EI)/((SQRT(EI)-SQRT(EFIN))**2)
        BETA=(((1+EX)-(1+2*EX)**U)/EX)
        RHO=(BETA*KZI/KT-SQRT(ABS(1-BETA*BETA))*KRHO/KT*COS(PHI))
        KT=1.0E+7*SQRT(2*EM*M*EFIN*E)/H
        KZF=KT*RHO
        KRHO=KT*SQRT(ABS(1-RHO*RHO))
        GO TO 460
C
C        CHANGE VALLEY PARAMETERS FOR INTERVALLEY PROCESSES.
C
430     IF(V.EQ.1) GO TO 440
        V=1
        EM=EM1
        GO TO 410
440     V=2
        EM=EM2
        GO TO 410
450     SS=SS+1
C
C        REGISTER SELF SCATTERING PROCESS.K SPACE POSITION UNCHANGED
C
        KZF=KZI
        KT=SQRT(KZF*KZF+KRHO*KRHO)
        EFIN=H*H*KT*KT*1.0E-14/(E*2*EM*M)
C
C        CHECK IF ELECTRON IS SCATTERED OUT OF MESH.IF SO,REGISTER
C        PROCESS ON COUNTER GMAX,AND PLACE ELECTRON ON EDGE OF MESH
C        LABEL 90 REPEATS ITERATIVE PROCESS STARTING WITH FREE
C        ELECTRON FLIGHT UNDER ELECTRIC FIELD.
C
460     IF(EFIN.LE.EMAX) GO TO 90
        GMAX=GMAX+1
        KT=1.0E+7*SQRT(2*EM*M*EMAX*E)/H
        IF(KRHO.GT.KT) KRHO=KT
        KZF=SQRT(ABS(KT*KT-KRHO*KRHO))
        GO TO 90
C
C        FINAL CALCULATION OF DRIFT VELOCITY-VEL,TIME SPENT IN EACH
C        VALLEY-VTIM(V),MEAN ENERGY-MNE
C
470     IF(IDIF.NE.0) GO TO 471
        VAVG=0.0
        V2AVG=0.0
        V3AVG=0.0
        V4AVG=0.0
471     IDIF=IDIF+1
        NPRINT=NPRINT+1
        ETOT=ETOT-((KZI*KZI-KZF*KZF)*10.0*H/(2*EM*M))
        KZTOT=KZTOT-ABS(KZI-KZF)
        KZI=KZF+(E*F(J)*1.0E+13/H)*((FT-TTCT)+TIME)
        ETOT=ETOT+((KZI*KZI-KZF*KZF)*10.0*H/(2*EM*M))
```

```
      KZTOT=KZTOT+ABS(KZI-KZF)
      VI=ETOT/KZTOT
      VAVG=(VAVG*(IDIF-1)+VI)/IDIF
      V2AVG=(V2AVG*(IDIF-1)+VI*VI)/IDIF
      V3AVG=(V3AVG*(IDIF-1)+VI*VI*VI)/IDIF
      V4AVG=(V4AVG*(IDIF-1)+VI*VI*VI*VI)/IDIF
      DIF=0.5 *FT*(V2AVG-VAVG*VAVG)
      DIF4=SQRT(ABS(V4AVG-4*V3AVG*VAVG+6*V2AVG*VAVG**2-3*VAVG**4)/12
     1.0)*FT
      CHECK=V3AVG-3*V2AVG*VAVG+2*VAVG**3
      ETOT=0.0
      KZTOT=0.0
      TTOT=0.0
      WRITE(5,430)F(J),VAVG,DIF,IDIF
      WRITE(7,430)F(J),VAVG,DIF,IDIF
  430 FORMAT(3(E9.3,1X),1X,I5  )
      NPRINT=0
      IF(IDIF.LT.NDIF) GO TO 87
      IDIF=0
      J=J+1
      IF(J.NE.NF+1) GO TO 30
      STOP
      END
```

APPENDIX 2

NUMERICAL DECOMPOSITION OF I-V CHARACTERISTIC AND
THE NOISE SPECTRAL DENSITY

For a given i, the sums in equations (9.5) and (9.6) can be written as

$$
V_{o_i} = \frac{\varepsilon A}{I_{o_i}} \int_{E_{L_1}}^{E_{L_2}} \frac{E^2 \mu_1 dE}{AN_D \mu_1 E} \left(1-q\frac{AN_D\mu_1 E}{I_{o_i}}\right) + \frac{\varepsilon A}{I_{o_i}} \int_{E_{L_2}}^{E_{L_3}} \frac{E^2 \mu_2 dE}{AN_D\mu_2 E}\left(1-q\frac{AN_D\mu_2 E}{I_{o_i}}\right) + \frac{\varepsilon A}{I_{o_i}} \int_{E_{L_i}}^{E_{L_{i+1}}} \frac{E^2 \mu_i dE}{AN_D\mu_i E}\left(1-q\frac{AN_D\mu_i E}{I_{o_i}}\right)
$$

(A.1)

$$
L = \frac{\varepsilon A}{I_{o_i}} \int_{E_{L_1}}^{E_{L_2}} \frac{E\mu_1 \, dE}{AN_D\mu_1 E}\left(1-q\frac{AN_D\mu_1 E}{I_{o_i}}\right) + \frac{\varepsilon A}{I_{o_i}} \int_{E_{L_2}}^{E_{L_3}} \frac{E\mu_2 dE}{AN_D\mu_2 E}\left(1-q\frac{AN_D\mu_2 E}{I_{o_i}}\right) + \frac{\varepsilon A}{I_{o_i}} \int_{E_{L_i}}^{E_{L_{i+1}}} \frac{E\mu_i dE}{AN_D\mu_i E}\left(1-q\frac{AN_D\mu_i E}{I_{o_i}}\right)
$$

(A.2)

Equations (A.1) and (A.2) can be rewritten as

$$
V_{o_i} = C_1 + \frac{\varepsilon A}{I_{o_i}} \int_{E_{L_i}}^{E_{L_{i+1}}} \frac{E^2 \mu_i dE}{N_D A\mu_i E}\left(1-q\frac{N_D A\mu_i E}{I_{o_i}}\right)
$$

(A.3)

103

$$L = C_2 + \frac{\varepsilon A}{I_{o_i}} \int_{E_{L_i}}^{E_{L_{i+1}}} \frac{E\mu_i dE}{(1 - q\frac{N_D A\mu_i E}{I_{o_i}})} \tag{A.4}$$

where

$$C_1 = \frac{\varepsilon A}{I_{o_i}} \sum_{s=1}^{i-1} \int_{E_{L_s}}^{E_{L_{s+1}}} \frac{E^2 \mu_s dE}{(1 - q\frac{AN_D\mu_s E}{I_{o_i}})} \tag{A.5}$$

and

$$C_2 = \frac{\varepsilon A}{I_{o_i}} \sum_{s=1}^{i-1} \int_{E_{L_s}}^{E_{L_{s+1}}} \frac{E\mu_s dD}{(1 - q\frac{N_D AE\mu_s}{I_{o_i}})} \tag{A.6}$$

Note that the subscripts for E_L have been shifted to avoid a subscript 0 for the computer.

Combining equations (A.3) and (A.4) after carrying out the integrals, we can express $E_{L_{i+1}}$ as a function of μ_i

$$E_{L_{i+1}}(\mu_i) = [E_{L_i}^2 + \frac{2qN_D}{\varepsilon} \cdot (C_1 - V_{o_i}) + \frac{1}{\mu_i} \frac{2I_{o_i}}{\varepsilon A} \cdot (L - C_2)]^{1/2} \tag{A.7}$$

Now we substitute $E_{L_{i+1}}(\mu_i)$ into equation (A.4)

$$L = C_2 + \frac{\varepsilon A}{I_{o_i}} \int_{E_{L_i}}^{E_{L_{i+1}}(\mu_i)} \frac{E\mu_i dE}{(1 - q\frac{N_D A\mu_i E}{I_{o_i}})} \tag{A.8}$$

We have to find the zero of the following function to find μ_i

$$F(\mu_i) = C_2 - L + \frac{\varepsilon A}{I_{o_i}} \int_{E_{L_i}}^{E_{L_{i+1}(\mu_i)}} \frac{E\mu_i dE}{(1-q\frac{N_D A\mu_i E}{I_{o_i}})} \qquad (A.9)$$

Carrying out the integral we have

$$F(\mu_i) = C_2 - L + \varepsilon A \left[\frac{E_{L_i}}{A_q N_D} - \frac{E_{L_{i+1}}}{A_q N_D} - \frac{1}{(A_q N_D)^2} \frac{I_{o_i}}{\mu_i} \ln \left(\left| \frac{1-qN_D A\mu_i E_{L_{i+1}}}{1-qB_D A\mu_i E_{L_i}} \right| \right) \right] \qquad (A.10)$$

A simple bisection method would have given the zeros of this function. However, in some cases the function $F(\mu_i)$ does not change sign and the bissection method becomes useless. This happened when $F(\mu_i)$ has a multiple root and the curve is just tangent to the μ_i-axis. In this case we have to check if the derivative of $F(\mu_i)$ changes sign and if the absolute value of $F(\mu_i)$ is close enough to zero. If these two conditions are met then we consider a possibility of having a zero in the neighborhood of that point.

The derivative of $F(\mu_i)$ is calculated by using Leibniz formula

$$\frac{\partial F}{\partial \mu_i} = \frac{\varepsilon A}{I_{o_i}} \int_{E_{L_i}}^{E_{L_{i+1}(\mu_i)}} \frac{\partial}{\partial \mu_i} \left[\frac{E\mu_i}{(1-q\frac{N_D \mu_i E}{I_{o_i}})} \right] dE + \frac{\partial E_{L_{i+1}}}{\partial \mu_i} \times \frac{\varepsilon A}{I_{o_i}} \left. \frac{E\mu_i}{(1-q\frac{N_D A\mu_i E}{I_{o_i}})} \right|_{E=E_{L_{i+1}}}$$

$$(A.11)$$

Once the μ_i and $E_{L_{i+1}}$ are found, D_i is easily calculated from equation (9.7)

$$S_{\Delta v_i}(f) = C_3 + \frac{4\varepsilon q A}{I_{o_i}^2} \int_{E_{L_i}}^{E_{L_{i+1}}} \frac{D_i(E_{L_{i+1}} - E)^2 \, dE}{(1 - q\frac{N_D A E \mu_i}{I_{o_i}})^3} \tag{A.12}$$

where

$$C_3 = \frac{4\varepsilon q A}{I_{o_i}^2} \sum_{s=1}^{i-1} \int_{E_{L_s}}^{E_{L_{i+1}}} \frac{D_s(E_{L_{i+1}} - E)^2 \, dE}{(1 - q\frac{N_D A E \mu_s}{I_{o_i}})^3} \tag{A.13}$$
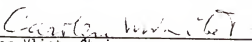
REFERENCES

1. R.R. Schmidt, "Noise and Current-Voltage Characteristics of Near-Ballistic GaAs Devices," Ph.D. Dissertation, University of Florida (1983)

2. M.S. Shur and L.R. Eastman, "Ballistic Transport in Semiconductor at Low Temperatures for Low-Power High Speed Logic," IEEE Electron Device Letters EDL-$\underline{1}$, 234 (1980)

3. M.S. Shur and L.R. Eastman, "Near Ballistic Electron Transport in GaAs Devices at 77.K," Solid-State Electron $\underline{24}$, 11 (1981)

4. J.J. Rosenberg, E.J. Yoffa, and M.I. Nathan, "Importance of Boundary Conditions to Conduction in Short Samples," IEEE Trans. Electron Devices ED-$\underline{28}$, 941 (1981)

5. A.J. Holden and B.T. Debney, "Improved Theory of Ballistic Transport in One Dimension," Electron. Letters $\underline{18}$, 558 (1982)

6. T.C. Fry, "The Thermionic Current Between Parallel Plane Electrodes; Velocities of Emission Distributed According to Maxwell's Law," Phys. Rev. $\underline{17}$, 441 (1921)

7. A. van der Ziel, M.S. Shur, K. Lee, T. Chen, and K. Amberiadis, "Carrier Distribution and Low-Field Resistance in Short n^+ n^- n^+ and n^+ p^- n^+ Structures," IEEE Trans. Electron Devices ED-$\underline{30}$, 128 (1983)

8. F.N. Hooge, T.J.G. Kleinpenning, and L.K. van Damme, "Experimental Studies on 1/f Noise," Report Progress in Physics $\underline{44}$, 479 (1971)

9. C.F. Whiteside, "Pulse Bias Noise Measurement," Master's Thesis, University of Florida (1982)

10. P.H. Handel, "1/f Noise an Infrared Phenomenon," Phys. Rev. Lett., $\underline{34}$, 1492 (1975)

11. F.N. Hooge, "1/f Noise is No Surface Effect," Phys. Lett. A $\underline{29}$, 139 (1969)

12. G. Kousik and C.M. Van Vliet, "Quantum 1/f Noise in Semiconductors and Metals Involving Acoustic, Optical, Polar Optical, and Impurity Scattering; Detailed Computation of the Hooge's Parameters," Invited Paper at the 8th International Conference on Noise in Physical Systems, Rome, Fall 1985

13. A. van der Ziel and C.M. Van Vliet," Mobility Fluctuation l/f noise in Non-uniform Non-Linear Samples and in Mesa Structures," Physica Status Solidi (a).$\underline{72}$, 453 (1982)

14. S. Tehrani, G. Bosman, and C.M. Van Vliet, "Space Charge Limited Current Noise in Presence of Traps in SiC," to be presented at the 8th International Conference on Noise in Physical Systems, Rome, Fall, 1985

15. V. Bareikis, A. Galdikas, R. Miliusyte, and V. Viktoravicius, Program and Papers of 5th Int. Conf. on Noise in Physical Systems (Bad Nauheim, W. Germany, March 1978), p. 212, Springer Verlag, Berlin

16. P.J. Price, "Monte Carlo Calculation of Electron Transport in Solids," Semiconductors and Semimetals, $\underline{14}$, 249 (1979)

17. W. Fawcett, A.D. Boardman, and S. Swain, "Monte Carlo Determination of Electron Transport Properties in Gallium Arsenide," J. Phys. Chem. Solids, $\underline{31}$, 1963 (1970)

18. C. Jacoboni and L. Reggiani, "Monte Carlo Method for the Solution of Charge Transport in Semiconductors with Applications to Covalent Materials," Rev. of Mod. Phys., $\underline{55}$, 645 (1983)

19. A.D. Boardman, Physics Programs, Vol. 4, Wiley Interscience Publications, New York (1980)

20. H.D. Rees, "Calculation of Stead State Distribution," Phys. Lett. A, $\underline{26}$, 416 (1968)

21. A. Gisolf and R.J.J. Zijlstra, "Scattering Noise of Hot Holes in Space-Charge Limited Current Flow in p-type S_i," J. Appl. Phys., $\underline{47}$, 2727 (1976)

22. G. Bosman, "Charge Transport Noise in Monocrystalline Silicon," Ph.D. Thesis, University of Utrecht (1981)

23. H. Kroemer, "Negative Conductance in Semiconductors," IEEE Spectrum, $\underline{5}$, 17 (1968)

24. P. Hesto, "Injection Dependence of Quasiballistic Transport in GaAs at 77K," Surf. Sci., $\underline{132}$, 623 (1983)

25. P. Hesto, J.F. Pone, and R. Castagne, "A Proposal and Numerical Simulation of N^+ N N^+ Schottky Device for Ballistic and Quasiballistic Electron Spectroscopy," Appl. Phys. Letters, $\underline{40}$, 405 (1982)

BIOGRAPHICAL SKETCH

Jean H. Andrian was born on February 16, 1955, in Tananarive, Madagascar. He graduated from Antsirabe High School in 1973. He then attended the University of Madagascar and obtained a diploma (DUES) in Mathematics in 1975. In 1976, he moved to Montreal, Canada, obtained his B.S. in electrical engineering in 1979 and his M.Sc. in engineering physics in 1981 at Ecole Polytechnique of Montreal. In 1981 he joined the Noise Research Laboratory at the University of Florida as a graduate research assistant. He is a member of Eta Kappa Nu Electrical Engineering Honor Society.

I certify that I have read this study and that in my opinion it conforms to acceptable standards of scholarly presentation and is fully adequate, in scope and quality, as a dissertation for the degree of Doctor of Philosophy.

C.M. Van Vliet, Chairperson
Professor of Electrical Engineering

I certify that I have read this study and that in my opinion it conforms to acceptable standards of scholarly presentation and is fully adequate, in scope and quality, as a dissertation for the degree of Doctor of Philosophy.

G. Bosman, Cochairperson
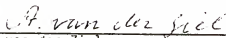Assistant Professor of Electrical Engineering

I certify that I have read this study and that in my opinion it conforms to acceptable standards of scholarly presentation and is fully adequate, in scope and quality, as a dissertation for the degree of Doctor of Philosophy.

E.R. Chenette
Professor of Electrical Engineering

I certify that I have read this study and that in my opinion it conforms to acceptable standards of scholarly presentation and is fully adequate, in scope and quality, as a dissertation for the degree of Doctor of Philosophy.

A. van der Ziel
Graduate Research Professor of
    Electrical Engineering

I certify that I have read this study and that in my opinion it conforms to acceptable standards of scholarly presentation and is fully adequate, in scope and quality, as a dissertation for the degree of Doctor of Philosophy.

S.S. Ballard
Distinguished Service Professor of Physics

This dissertation was submitted to the Graduate Faculty of the College of Engineering and to the Graduate School, and was accepted as partial fulfillment of the requirements for the degree of Doctor of Philosophy.

May 1985

_____
Dean, College of Engineering

_____
Dean, Graduate School